PHOTONICS Research

Cavity engineering of two-dimensional perovskites and inherent light-matter interaction

Shuai Zhang,[1,2] Yangguang Zhong,[1] Fan Yang,[1,3] Qinxuan Cao,[1,4] Wenna Du,[1] Jianwei Shi,[1] and Xinfeng Liu[1,2,*]

[1]CAS Key Laboratory of Standardization and Measurement for Nanotechnology, CAS Center for Excellence in Nanoscience, National Center for Nanoscience and Technology, Beijing 100190, China
[2]University of Chinese Academy of Sciences, Beijing 100049, China
[3]Department of Chemistry, School of Science, Tianjin University, Tianjin 300072, China
[4]School of Materials Science and Engineering, Zhejiang University, Hangzhou 310027, China
*Corresponding author: liuxf@nanoctr.cn

Received 23 June 2020; revised 22 August 2020; accepted 7 September 2020; posted 8 September 2020 (Doc. ID 400259); published 30 October 2020

Two-dimensional (2D) perovskites are hybrid layered materials in which the inorganic lattice of an octahedron is sandwiched by organic layers. They behave as a quantum-well structure exhibiting large exciton binding energy and high emission efficiency, which is excellent for photonic applications. Hence, the cavity modulation and cavity devices of 2D perovskites are widely investigated. In this review, we summarize the rich photophysics, synthetic methods of different cavity structures, and the cavity-based applications of 2D perovskites. We highlight the strong exciton–photon coupling and photonic lasing obtained in different cavity structures. In addition, functional optoelectronic devices using cavity structures of 2D perovskites are also reviewed.

https://doi.org/10.1364/PRJ.400259

1. INTRODUCTION

The pursuit of novel optical-electrics with fast operation and small size requires the efficient control of light propagating at nanoscale. A microcavity provides a place where light can be directed with few propagation losses and a relatively long lifetime, which can be depicted as a quality (Q) factor. More importantly, the confined photons can interact with matter. The internal dissipative mechanisms, such as spontaneous emission, can be coupled with resonant optical modes. This leads to the observation of accelerated emitting dynamics, local field enhancement (Purcell effect) [1], and a variety of applications, such as light-emitting diodes (LEDs) and semiconductor lasers. If the coupling between optical modes and matter overcomes their loss, the quantum entanglement between them becomes possible, and the strong coupling between light and matter can be established. The new quasi-particle—polaritons, exhibiting the extremely light effective mass and notable nonlinearity from their light and matter part, bring fantastic polaritonic effects such as slow light, Bose–Einstein condensation (BEC), and low threshold polariton lasers [2].

To obtain efficient light harvesting for optical-electric devices, the choice of active materials for light emission and propagation has been investigated for a long time, including traditional inorganic materials, quantum-well (QW) materials, and organic dyes [3]. In recent years, lead halide perovskites have become favored materials not only for solar cells [4], but also for photon detectors [5] and light emission devices [6] such as LEDs and microlasers. They behave with a high absorption coefficient [7], long diffusion length [8], high defect tolerance [9], and low rates of nonradiative recombination [10]. The typical chemical formula can be expressed as ABX_3, where A is a monovalent organic or inorganic cation (Cs^+, Rb^+, $CH_3NH_3^+$, $NH_2CH{=}NH_2^+$, etc.), B is a metal cation (Pb^{2+}, Sn^{2+}, Ge^{2+}, etc.), and X is a halide anion (Cl^-, Br^-, I^-, or their mixture). The typical three-dimensional (3D) structure consists of an octahedral cluster $[BX_6]^{4-}$ and A cations at eight corners [Fig. 1(a)]. However, when the organic cations are too large to place among the octahedral cluster, they have to be sandwiched between two $[BX_6]^{4-}$ octahedral cluster layers because of steric effects [Fig. 1(b)]. Here perovskites behave as a two-dimensional (2D) layered structure with the chemical formula of R_2BX_4. The large dielectric contrast between inorganic and organic layers makes 2D perovskites a kind of QW structure [11]. The inorganic layers connected via coulombic interactions act as "wells" and are barriered by hydrophobic, insulating organic layers, leading to a periodic thickness of up to a few nanometers [12] and strong quantum confinement. After the early works of layered perovskites containing single

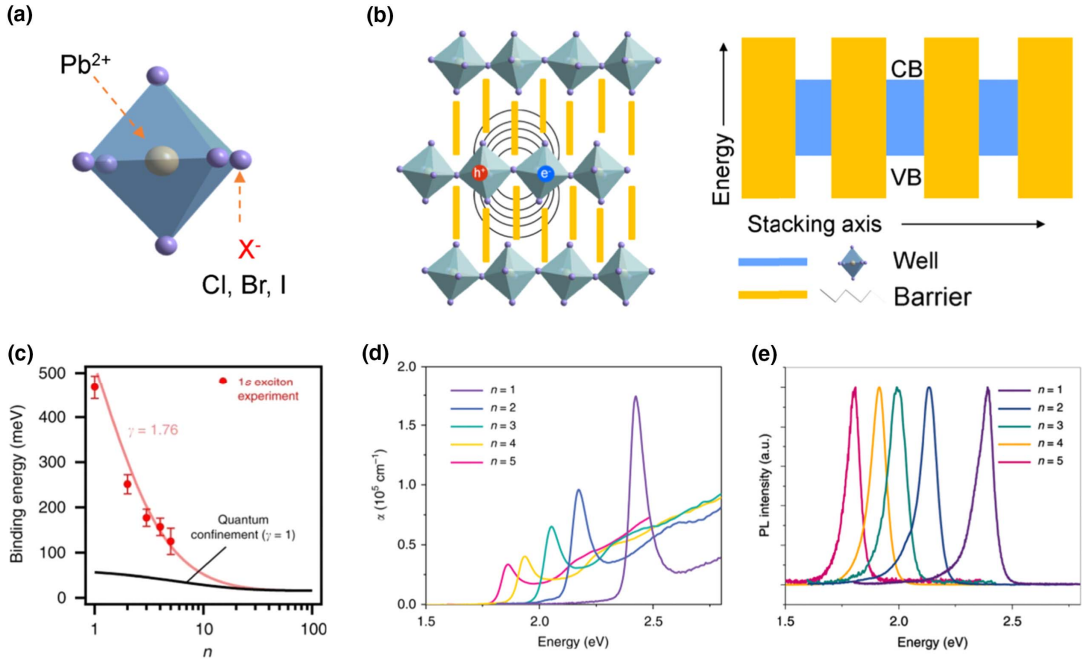

Fig. 1. Crystal structure and layer-dependent excitonic properties of 2D perovskite. (a) Fundamental unit of octahedral inorganic framework $[PbX_6]^{2-}$, where X = Cl, Br, I; (b) crystal structure of 2D layered perovksite. The inorganic layers are surrounded by insulative organic layers, resulting in self-assembled multiple quantum-well structures, where interlayer organic cations provide both dielectric and quantum confinement for inorgaic stacks. (c) The exciton binding energy of 2D perovskite decreases with inorganic layer number as a result of weak quantum confinement at large inorganic layer numbers [13]. Copyright 2018, Springer Nature. (d) and (e) are the absorpation and PL spectra of 2D perovskite $(BA)_2(MA)_{n-1}PbnI_{3n+1}$ at different n values [14]. Copyright 2020, Springer Nature.

inorganic layer ($n = 1$) in a well, more research has centered on various inorganic layers ($n > 1$) with the chemical formula of $R_2A_{n-1}B_nX_{3n+1}$. The additional small organic cation (A) is to form the multilayered "quasi-2D" perovskites with distinct quantum confinements at different n values. The flexible tunability of n values has a great influence on the exciton binding energy and bandgap because of the well thickness and dielectric environment [Fig. 1(c)] [13]. Therefore, 2D perovskites have unprecedented controlling ways for optical absorption [Fig. 1(d)] and colorful light emission [Fig. 1(e)] [14], including halogen alloying, structure and dielectric control by organic components, and inorganic layer thickness. The engineering of 2D perovskites is thus advantageous for light-emitting applications over the visible and near-infrared spectral region [15].

In the past few years, 2D perovskites have been the subject of fast development in cavity-based applications and fundamental studies. Due to the large exciton binding energy and oscillation strength, strong exciton–photon coupling has been observed in 2D perovskite single-crystal, Fabry–Perot (F-P) cavities, and photonic crystal structures at room temperature [16]. In addition, 2D perovskites are promising optical gain media so that lasing from 2D perovskite microstructures such as inhomogeneous thin films [17] and mechanically exfoliated plates [18] have been reported. Compared to the 3D perovskites, 2D perovskites behave with improved environmental stability and exciton confinement [11], which are more favorable for efficient LEDs and lasers. Additionally, large surface, ultrathin film can be easily exfoliated from the bulk crystal or grown by solution methods [19], which is essential for nanosized cavity devices. As a layered structure, it is very similar to the transitional metal dichalcogenide (TMD) materials. Considering the low photoluminescence quantum yield (PLQY) of TMD materials, the value of which in ABX_2 (A = Mo, W; B = S, Se.) is below 1% [20], the much easier fabrication and better excitonic emission efficiency [21–23] make 2D perovskites more advantageous active materials than TMD materials. Finally, the unique structures of these hybrid layered materials induce rich structure-related anisotropic emission behaviors, which may make 2D perovskite-based optical cavities the basis of novel functional devices with enhanced performance, such as photodetectors, solar cells, LEDs, light modulators, and nonlinear photonic devices [24–27].

Hence, this review captures the unique optical performance of 2D perovskites inside the optical cavities, discusses the fundamental photon physics, and summarizes the potential applications of 2D perovskite-based cavities. Since 2D perovskites have infinite tunability as discussed above, we first discuss the structure-related optoelectronic properties, including the impacts of a dielectric environment and structure order/disorder. Second, we review the growing methods of 2D perovskite and integration to optical cavities, including self-organized structures, vertical F-P cavities, and periodical cavity structures. Later, we discuss the light-matter interaction and applications of 2D perovskite-based cavities, including strong exciton–photon coupling and photonic laser and function devices. Finally, we discuss the challenges and limitations of the

current performance of cavity applications and propose future directions.

2. STRUCTURE-RELATED OPTOELECTRONIC PROPERTIES

A. Low Trap States and High Quantum Yield

Quantum yield is an important parameter in LEDs and lasers. To obtain high quantum yield, one would improve the rate of radiative recombination by excitonic recombination and bimolecular recombination or reduce the nonradiative recombination. Ramirez *et al.* reported the highly luminescent 2D perovskite $(PA)_2(MA)_2Pb_3Br_{10}$ (PA = propylamine, MA = methylamine) [28], with the quantum yield of 29.6%, which is much higher than the counterpart $MAPbBr_3$—the value is 3.6% [Fig. 2(a)]. It shows a blueshifted and less well-defined absorption edge. Power-dependent photoluminescence (PL) spectra reveal a power-law function with the slope of 1.037, an indication of an exciton radiative recombination and low trap density [29]. The QW structure of 2D perovskites makes their exciton binding energy much higher than their 3D counterparts, and contributes to the more excitonic emission character, which is more efficient for radiative recombination. In contrast, the excitons in 3D perovskite are more easily ionized into free carriers, and the charge-carrier trapping reduces the PL emission [30]. The quantum yield of 2D perovskite can be further improved to 80% by surface passivation [31], which is able to reduce the nonradiative recombination by surface state.

B. Large Optical Anisotropies

2D materials usually present optical anisotropies due to the structural inhomogeneities at different crystal axes [32], which is also applicable to 2D perovskites where carriers are considered to be confined at the inorganic layers. By using a polarized Fourier-resolved PL measurement, Fieramosca *et al.* observed that 2D perovskites have both in-plane components and out-of-plane components of excitons, in which the out-of-plane excitonic emission is observed at the total internal reflection (TIR) angle of a TM section [33]. In contrast, MoS_2 with full in-plane excitons, behaves as vanishing emissions at this angle. By using different organic ligands and the same inorganic layers, the component of out-of-plane excitons can be further varied from 10% to 18%, which also reveals the barrier-dependent exciton oscillating out of the inorganic layers plane. Later, Decrescent *et al.* investigated the optical constants of both the in-plane and out-of-plane by using the momentum-resolved optical spectra [Fig. 2(b)] [34]. The result can be well understood by dielectric inhomogeneity rather than the electronic states of inorganic layers, which also suggests the significant tuning of optical anisotropies by varying the organic cation.

C. Carrier–Phonon Coupling

Compared to conventional semiconductor QWs with relatively low binding energy, 2D perovskites exhibit distinct features, such as more stable excitons at room temperature. More importantly, the ionic character and the "softness" of the lattice result in carrier scattering by coupling to phonons [35]. Recent studies of vibrational spectra reveal that excitons can be coupled to a series of phonon modes, and the coupling modes can be tuned by the organic cation and thickness of the inorganic layers. The low energy longitudinal optical (LO) phonons of 8–17 meV [36–38] and 12–14 meV [38,39] can be resolved by ultrafast transient absorption (TA) spectroscopy. Coherent coupling with LO phonons can be observed by high-resolution resonant impulsive stimulated Raman spectroscopy using an ultrashort pump pulse [Fig. 2(c)] [40]. Additionally, coherent longitudinal acoustic (LA) phonons coupled with hot excitons have also been observed in 2D perovskites. They propagate along the cross-plane direction of 2D perovskites, and the group velocity and propagation length can be varied by the perovskite layer thickness [41]. Generally, carrier–phonon coupling results in fast nonradiative decay, and lowers the PL quantum yield. Reduction of molecular motion by varying the organic ligands in 2D perovskites could be possible for better optoelectronic performance [42].

D. Lattice Distortion and Self-Trap States

Structure distortion can be caused and stabilized by the local potential well induced by exciton itself, resulting in a low energy, broadband white-light emission, which is called a self-trapped exciton [Fig. 2(d)]. These phenomena have been observed in layered Pb-Br perovskite of different structure types [43]. At room temperature, they behave as narrow blue PL and small Stokes shift and are assigned to free excitonic emission. At low temperature, a new broad PL band with a large Stokes shift arises, which has been attributed to self-trapped exciton emission. Cortecchia *et al.* reported the origin of structural distortion in $(EDBE)PbI_4$ [EDBE = 2, 2-(ethylenedioxy)bis (ethylammonium)] where the large deformation of the Pb-I bond length and I-Pb-I bond angles can result in self-trapped states [44]. Self-trapped states can be established from free exciton by electron–phonon coupling with an ultrafast time scale of subpicoseconds or picoseconds, which can be distinguished from defect-induced traps [45].

3. FABRICATION OF CAVITY STRUCTURES AND MATERIAL SOURCE

In an optical cavity, light is confined and resonant-recycled with a certain photon energy and group velocity. The most common type of optical cavity is the F-P cavity, where light oscillates between two end facets of the longitudinal direction. The mode wavelength spacing of the light $\Delta\lambda$ can be expressed as [46]

$$\Delta\lambda = \frac{\lambda^2}{2L[n - \lambda(\mathrm{d}n/\mathrm{d}\lambda)]}, \tag{1}$$

where n is the refractive index, L is the cavity length, and $n - \lambda(\mathrm{d}n/\mathrm{d}\lambda)$ is the group refractive index n_g. Another type of cavity is the whispering-gallery mode (WGM) cavity, where light can travel along the side faces of the cavity, providing that total internal reflection is reached. The shape of this cavity can be varied from square or hexagon plates, round disks, spheres, etc. The spectral spacing $\Delta\lambda$ has the relationship with round-trip distance L as [47]

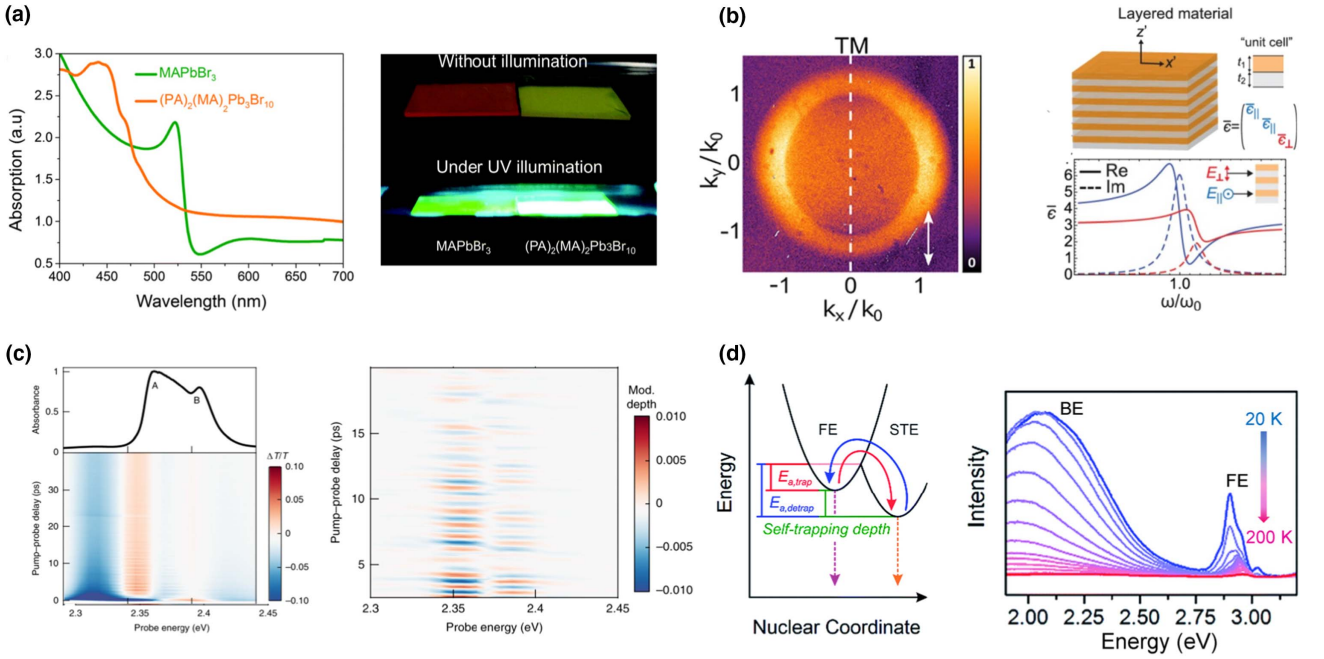

Fig. 2. Unique excitonic behaviors of 2D perovskite. (a) Left, absorpation spectra of $(PA)_2(MA)_2Pb_3Br_{10}$ and $MAPbBr_3$ thin films; right, optical images of the two perovskite thin films under UV illumination. Adapted from [28] with permission from Royal Society of Chemistry. (b) In-plane and out-of-plane exciton of 2D perovskite. Left, 2D Fourier image of PL in the vertical polarization (white arrow), in which out-of-plane component locates at the TIR angle (k_0). Adapted with permission from [33]. Copyright 2018, American Chemical Society. Right, dielectric model of 2D perovskite indicating the in-plane and out-of-plane electric field. Adapted with permission from [34]. Copyright 2019, American Chemical Society. (c) Phonon coherence of $(PEA)_2PbI_4$. Left, absorpation and time-resolved differential transmission spectrum at 5 K; right, oscillatory components extracted from the time-resolved differential transmission spectrum indicating the coherent vibrational dynamics. Adapted with permission from [40]. Copyright 2019, Springer Nature. (d) Energy diagram showing the generation of free exciton and self-trapped exciton due to the lattice reorganization; the resulting emission spectra behave as sharp excitonic emission and broad exciton self-trapping emission at low temperature. Adapted from [43]. Published by the Royal Society of Chemistry.

$$\Delta\lambda = \frac{\lambda^2}{n_g L}. \tag{2}$$

In addition, periodic dielectric nanostructures such as 2D photonic crystals [48] and distributed Bragg reflectors (DBRs) [49] are also used as optical cavities to control the propagation of light at arbitrary designed angles. The internal elements are usually periodically separated at half the wavelength of the light.

2D perovskites can be easily prepared in the types of single crystals [50,51], nanocrystals [52], microstructures [53], and thin films [54] using chemical vapor deposition (CVD), anti-solvent methods, or just spin coating on a substrate [55]. So far, these types of 2D perovskites have been widely used as active materials of different optical cavities, as mentioned above (Fig. 3). Based on the morphology of different material sources and desired optical performance, we discuss the different cavity structures as three species, i.e., self-assembled crystal cavities, structure-templated cavity arrays, and vertical F-P cavities. Table 1 shows the optical performance of different cavities of 2D perovskite, highlighting the materials sources and Q factor of different cavity structures. The details are discussed below.

Table 1. Optical Performance of 2D Perovskite-Based Microcavities

Cavity Types	Active Materials	Working Wavelength	Cavity Q	Application	Ref.
Self-assembled crystal cavity					
	$(PEA)_2PbBr_4$ sheet	415–430 nm	379–1045	Strong coupling	[56]
	$(BA)_2(MA)_2Pb_3I_{10}$ thin flake	620–635 nm	528–903	Lasing	[18]
	$(BA)_2(MA)Pb_2I_7$ bulk crystal	578 nm	1155	Lasing	[57]
Vertical F–P cavity					
	$(PEA)_2PbI_4$ thin film	517 nm	25	Strong coupling	[58]
		564 nm	86	Strong coupling	[59]
	$(PEA)_2PbI_4$ flake	530–575 nm	2200	Strong coupling	[60]
	$(PEA)_2Cs_2Pb_3I_{10}$ microcrystal	532–539 nm	665	Lasing	[17]
Cavity array					
	$(PEA)_2PbI_4$ thin film in air hole	537 nm	222	Strong coupling	[61]
	$(BA)_2(MA)_5Pb_6I_{19}$ in PDMS template	541–547 nm	2600	Lasing	[62]

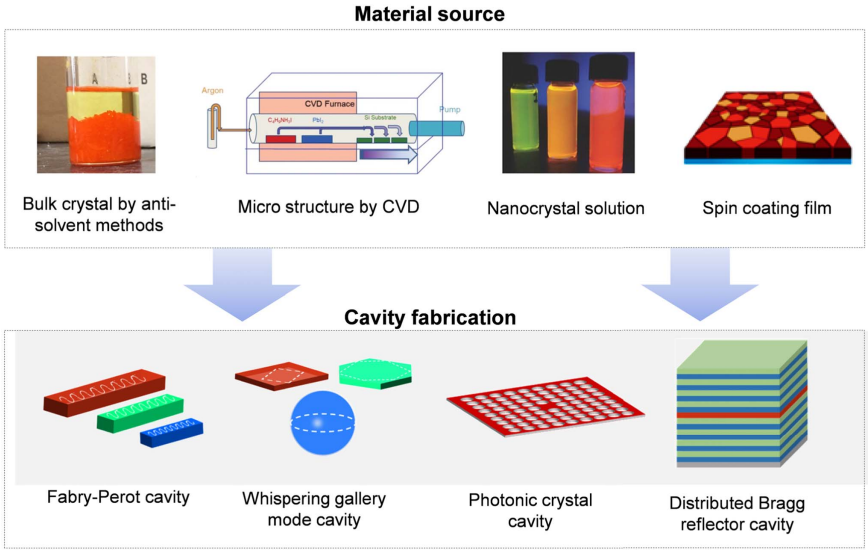

Fig. 3. Fabrication of different 2D perovskite photonic cavities. Upper side shows the synthesis of 2D perovskite materials with different morphology, including bulk crystals, microstructures, nanocrystals, and thin films. From left to right, the first image is adapted with permission from [64]. Copyright 2016, American Chemical Society. Further permissions related to the material excerpted should be directed to the ACS. The second image is adapted with permission from [53]. Copyright 2019, John Wiley and Sons. The third image is adapted with permission from [52]. Copyright 2015, John Wiley and Sons. The fourth image is adapted from [54]. Published by MDPI. Bottom side summarizes the different cavity structures including F-P cavity, WGM cavity, photonic crystal cavity, and DBR cavity.

A. Self-Assembled Crystal Cavities by 2D Perovskite Nano/Microstructures

Owing to the high reflectivity of perovskites with different shapes, the single particle of perovskites itself can be a self-organized optical resonator [63]. Perovskite microstructures such as nanowires or nanoplates can be used as F-P cavities or WGM cavities, which can be directly obtained by solution methods or CVD without further lithography or etching processes.

As a kind of layered material, 2D perovskites micro/nanoplates can be mechanically exfoliated from their bulk crystal with a large and flat surface. The bulk crystals are usually obtained by liquid phase crystallization. The dissolved lead halide and organic amine halide are mixed together at high temperature. The crystal growth can be controlled by cooling down at a certain rate or evaporating the solvent at a slow rate. Stoumpos *et al.* reported $(BA)_2(MA)_{n-1}Pb_nI_{3n+1}$ (BA = butylammine, $n = 1$–4) by adding the neutralized BA into the mixed hot solution of HI, H_3PO_2, PbO, and further cooling down the mixture to room temperature [64]. Leng *et al.* also synthesized centimeter-sized single-crystal 2D perovskites $(BA)_2(MA)_{n-1}Pb_nI_{3n+1}$ ($n = 1$–4) by a temperature-programmed crystallization method [65]. Evaporating the solvent slowly can be easier and cleaner for obtaining high-quality single crystals, such as the systemization of $(HA)_2PbI_4$ (HA = n-hexylamine) by slowly evaporating the acetone solvent [66] and $(BA)_4Pb_3I_4Br_6$ by slowly evaporating N, N-dimethylformamide [67], but is a time-consuming method.

Although mechanical exfoliation is a convenient way to obtain microstructures of 2D perovskites with different widths and thicknesses, the shape is uncontrollable and is challenging for reliable modulation of light in the cavity. Dou *et al.* obtained atomically thin, uniform square-shaped 2D perovskite $(BA)_2PbBr_4$ by evaporating the mixed solution of BABr and $PbBr_2$ in the cosolvent of dimethylformamide (DMF) and chlorobenzene (CB) at 75°C for 10 min [68]. Shi *et al.* further reported the synthesis of highly stable, square-shaped 2D perovskite lateral epitaxial heterostructures by two steps of crystallization of 2D perovskite precursor solution [69]. The formation of large 2D halide perovskite sheets was controlled by evaporating the antisolvent of CB. Ma *et al.* reported that 2D perovskite rectangular microplates and nanowires can be directly obtained by a novel solution method named as the dissolution–recrystallization process [70]. They synthesized $(PEA)_2PbX_4$ (PEA = phenethylamine, X = Br and I) by placing a lead acetate film into the PEAX solution in isopropanol for a specified time, further washed away the solution, and dried the substrate. The obtained microplates and nanowires have a typical size of tens of micrometers and thickness of hundreds of nanometers. Another method to grow structured semiconductors is CVD. It is a scalable approach for the growth of 2D TMDs and can be applied to the growth of 3D perovskite. The CVD growing of 2D perovskites has been explored by Ghoshal *et al.* [53]. They developed a low-temperature vacuum-assisted chemical vapor deposition (LTCVD) method to grow $(C_4H_9NH_3)_2PbI_4$. Briefly, lead iodide and n-butylammonium iodide are heated at the temperature of 400°C for 10 min with argon of 30 sccm and pressure of 600 mTorr. Based on the concentration and depending on the distance between material source and substrates, different growth processes form the morphology of nanoplatelet or nanowires with lengths from several to tens of micrometers.

B. Periodic and Photonic Crystal Cavities by Structure-Templated 2D Perovskite

Reproducible photonic arrays are demanded for integrated information transmission and the mass production of photonic

devices, which is still challenging by direct growth of photonic nanostructures such as nanowires and nanoplates. Solution processability ensures the direct fabrication of cavity arrays by casting perovskite solution onto a periodical structure such as SiO_2 etching hole lattices and Ag gratings [62,71]. This convenient method, however, often results in disordered grain boundary and reducing quantity factor of cavity structures. Miscibility of perovskite with organic matrix materials [72,73] provides another avenue of emitted cavity array by engineering the shape of perovskite-embedded organic matrix materials. Compared with solution-processed thin film, this method can produce cavities of different shapes with a flat surface and a homogeneous distribution of perovskite. The flexibility has been proved in 3D perovskite by embedding $CsPbBr_3$ nanocrystals (NCs) with poly-(methylmetacrylate) (PMMA) [74] or polyacrylonitrile (PAN) [75]. Comparatively, 2D perovskites behave with improved flexibility and deformable properties due to the organic layers [76]. Zhang *et al.* designed the 2D perovskites nanowire and microring arrays by a polydimethylsiloxane (PDMS) template that confined solution growth of 2D perovskites [61,77]. Initially, the PDMS templates were fabricated by casting PDMS against the silicon mother-molds of microrings or nanowires by photolithography. By pressing the PDMS templates onto the top of stock solution containing BABr, MABr, and $PbBr_2$, the nucleation of 2D perovskites can occur inside the PDMS templates, and the PDMS-templated 2D perovskite cavity arrays can be obtained. The direct nucleation from comixing the precursor solution, however, often induces the formation of multiple phase 2D perovskites with different inorganic layer numbers, which is widely observed in spin-coating film of 2D perovskites. To obtain the structure templated cavity with a pure phase of desired inorganic layer number, one would consider the synthesis of 2D perovskite colloidal NCs with a single emission peak. Chang *et al.* reported the synthesis of $(BA)_2(MA)_{n-1}Pb_nI_{3n+1}$ ($n = 1$–5) quantum dots (QDs) with an average size of 10 nm at room temperature [22]. By adjusting the ratio of MAX and PbX_2 in the precursor solution before its being dropped into a quenching solvent chlorobenzene, well-dispersed perovskite QDs with different n values were obtained. Upon increasing the n value, the PL spectra of these QDs show a redshift and low FWHM of 11–21 nm, suggesting highly pure 2D perovskite QDs. In addition, they are more optically stable than 3D perovskite QDs, which makes them an advantageous gain medium for structure-templated cavities.

C. Vertical F–P Cavities Containing 2D Perovskite Thin Film or Single Crystals

A vertical F–P cavity means that the F–P oscillation modes are perpendicular to the plane of active material. It consists of two strictly parallel mirrors separated by the active material. The reflectivity of the two mirrors has a great impact on the cavity loss and Q factor. Metallic mirrors behave as the constant reflectivity of a broad wavelength, which may not be suitable for the transmission of light at certain wavelengths. Bragg mirrors can also be used as mirror pairs of an F–P cavity, which is equivalently called the DBR cavity. A Bragg mirror is produced by periodically stacking a quarter-wave thickness of two dielectric materials with different refractive indices, resulting in ultrahigh reflectivity at the designed wavelength [78]. In a typical DBR cavity, two Bragg mirrors are sandwiched by a gain medium, resulting in a vertical F–P cavity mode across the gain medium. If the resonance energy of the vertical F–P cavity is within the high-reflectivity energy region of two Bragg mirrors, the DBR cavity with a high Q factor can be established [79]. Early work on 2D perovskite-embedded vertical F–P cavities usually used a solution-processed 2D perovskite thin film as the gain medium between Bragg mirrors and a metal surface, which behave at the low Q factor of 25 [80,81]. A higher Q factor of 86 was later obtained in a two-Bragg-mirror structure containing 60 nm of spin-coated $(PEA)_2PbI_4$ film [59]. The Q factor can be further improved by using a 2D perovskite single-crystal structure as the gain medium inside two Bragg mirrors. For example, Wang *et al.* fabricated a DBR cavity containing $(PEA)_2PbX_4$ (X = Br, I) bulk crystal and a high Q factor of 2200 [60]. 2D perovskite-embedded DBR cavities have witnessed the strong exciton–photon coupling and vertical cavity surface-emitting lasers (VCSELs) at room temperature.

4. LIGHT-MATTER INTERACTIONS AND OPTOELECTRONIC APPLICATIONS OF 2D PEROVSKITE CAVITY STRUCTURES

2D perovskites exhibit unique optical properties, combining the advantage of atomic thin 2D materials and the high quantum efficiency of perovskite, as discussed in Section 2. Moreover, the ease of fabrication and integration with different optical cavities makes 2D perovskites attractive active materials for various photonic applications. In optical cavities, the excitonic transition of a semiconductor can be coupled to the external optical field. Based on the architecture of the cavities and the excitation conditions, the light-matter interaction can be in the strong coupling region or weak coupling region. Consequently, various optical performances and optoelectronic applications of 2D perovskites can be expected, such as exciton–polariton, lasing, and functional devices of different photonic structures.

A. Strong Exciton–Photon Coupling of 2D Perovskite Cavity Structures

The establishment of strong exciton-photon coupling requires the robust exciton to be well overlapped with the antinode of the optical field inside a cavity [3]. A typical structure is shown in Fig. 4(a), in which the active material is inserted between two mirrors, and excitons are coupled with the F–P cavity mode. The resulting quasi-particle, exciton polariton behaves as two separating energy branches named as upper polariton branches (UPBs) and lower polariton branches (LPBs) in a dispersion curve [Fig. 4(b)], which stems from the crossed dispersion of exciton E_X and cavity mode E_C. The dispersion relation of the two polariton branches can be expressed as

$$E = \frac{1}{2}\left(E_C + E_X \pm \sqrt{\Delta^2 + \Omega^2}\right), \tag{3}$$

in which $\Delta = E_C - E_X$ is the detuning energy, and Ω is the Rabi splitting, related to the coupling strength of the exciton and photon [2].

Traditional III–V and II–VI semiconductors such as GaAs and ZnTe were initially demonstrated as exciton–photon coupling [82–85]. Their QW structures exhibit a narrow exciton

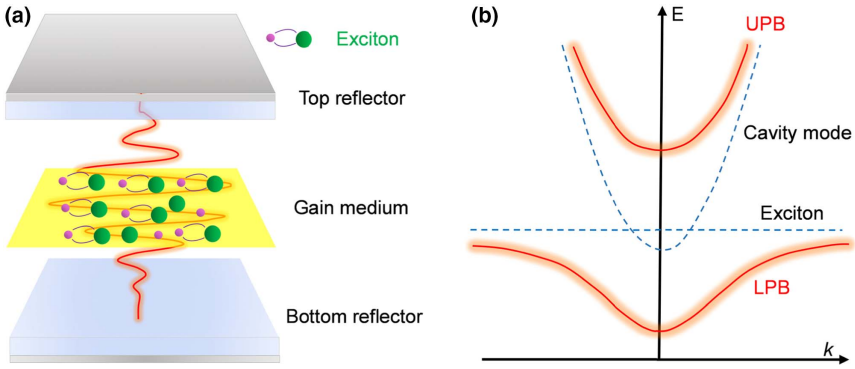

Fig. 4. Model of exciton polariton inside a cavity. (a) Schematic diagram showing the strong coupling of excitons in the gain medium and F–P cavity mode between two reflectors; (b) dispersion curve of exciton polariton consisting of two polariton branches. The dashed lines are uncoupled exciton and cavity modes.

linewidth and a large exciton Bohr radius, indicating low loss and sizeable nonlinear interaction with polaritons [3]. However, their weak exciton binding energy restricts the operating temperature to below 100 K. Wide bandgap inorganic materials such as GaN and ZnO possess large exciton binding energy (45–60 meV) and oscillator strength, making the polariton operation at room temperature necessary [86,87]. The intrinsic small exciton Bohr radius of these materials indicates weak exciton–exciton interaction, which is a drawback because the nonlinear polariton interaction is hindered [88]. A similar situation also exists in organic dyes and polymers with Frenkel excitons [89].

Metal-halide perovskites have been considered competitive materials for room temperature polaritons due to their large exciton binding energy and high quantum yield [10,90]. In the past several years, room temperature exciton polaritons [91–94] and polariton condensation [92,95,96] have been demonstrated in 3D perovskite [97]. Continuous-wave pumped lasers have also been reported in $CsPbBr_3$ nanowires due to the large refractive index induced by the exciton–polariton effect [98,99]. The investigation of exciton–polariton in 2D perovskites with much higher binding energy is essentially much earlier. Due to the ease of the solution process, most of the early work was focused on the polycrystalline film coupled with different cavities, which often results in a low Q factor [81,100,101]. The investigation is accelerated along with the pursuit for high-quality cavity structure, leading to the observation of attractive polariton effects that are different from their 3D counterparts [33,102]. 2D perovskites coupled with different cavity structures are reviewed below.

1. Exciton–Polariton in Self-Assembled Crystal Cavities of 2D Perovskite

Fieramosca *et al.* reported the first observation of exciton polaritons in 2D perovskite single-crystal flakes [33]. Light inside the single crystal of 2D perovskites can be a self-assembled cavity in which light can oscillate between two smooth interfaces of a single crystal or propagate along the plane of the flake [Fig. 5(a)]. The latter was verified by the PL image in Fig. 5(b). Apart from the bright spot representing the excitation region, the bright boundary of flakes is induced by the leakage of guided light at the edges of the flake because light can propagate for tens of microns without being scattered by defects. Polarization-dependent and angle-resolved reflection spectra indicate the strong coupling of multi-F–P modes with either in-plane or out-of-plane oscillating dipoles when close to the excitonic resonance. Moreover, by increasing the length of the organic ligand, the out-of-plane oscillator strength is weakened. The observations suggest the organic interlayer plays a significant role in the anisotropy of the exciton and exciton polariton, rather than a passive insulating barrier. Later, they observed the blueshift of polariton modes in single crystals of 2D perovskites $(PEA)_2PbI_4$, which is related to polariton nonlinearity [102]. By injecting a linearly polarized laser beam beyond the crystal–air TIR angle [green region in Fig. 5(c)], the blueshift of two LPBs (LP1, LP2) is characterized by increasing the incident power. The LP1, with more excitonic fraction, behaves with a larger blueshift, which confirms the inherent excitonic interaction with the interaction constant $g_x \sim 1 \pm 0.2\ \mu eV \cdot \mu m^2$ per inorganic layer. This value is much higher than the value in organic excitons and is comparable with the value estimated for a GaAs QW [103]. In another type of 2D perovskite $(PEA)_2PbBr_4$, Zhang *et al.* reported exciton polaritons with Rabi splitting of ~259 meV in a millimeter-sized single crystal sheet [56]. By the microregion PL measurement at different sites of the 2D perovskite sheet, they found the enhanced PL emission from the edge of the sheet exhibiting F–P mode oscillation. The mode spacing is reduced when approaching the excitonic resonant energy, in indication of strong exciton–photon coupling. The oscillating mode energies in energy-wave vector coordinates can be well fitted by a coupled oscillator model describing the strong coupling of light and matter [104]. A sensitive detection of the F–P oscillation is realized in 2D perovskite sheets with an extremely smooth top surface and both edges. In the bottom of Fig. 5(d), the PL mapping of the selected area overlaps with an evident interference pattern, which concludes as the oscillating modes are induced by the exciton–photon coupling.

2. Exciton–Polariton in 2D Perovskite-Embedded Vertical F–P Cavities

Deleporte's group demonstrated the first vertical F–P cavity containing 2D perovskite $(PEA)_2PbI_4$ thin film between a dielectric mirror and a silver mirror [80]. The strong coupling

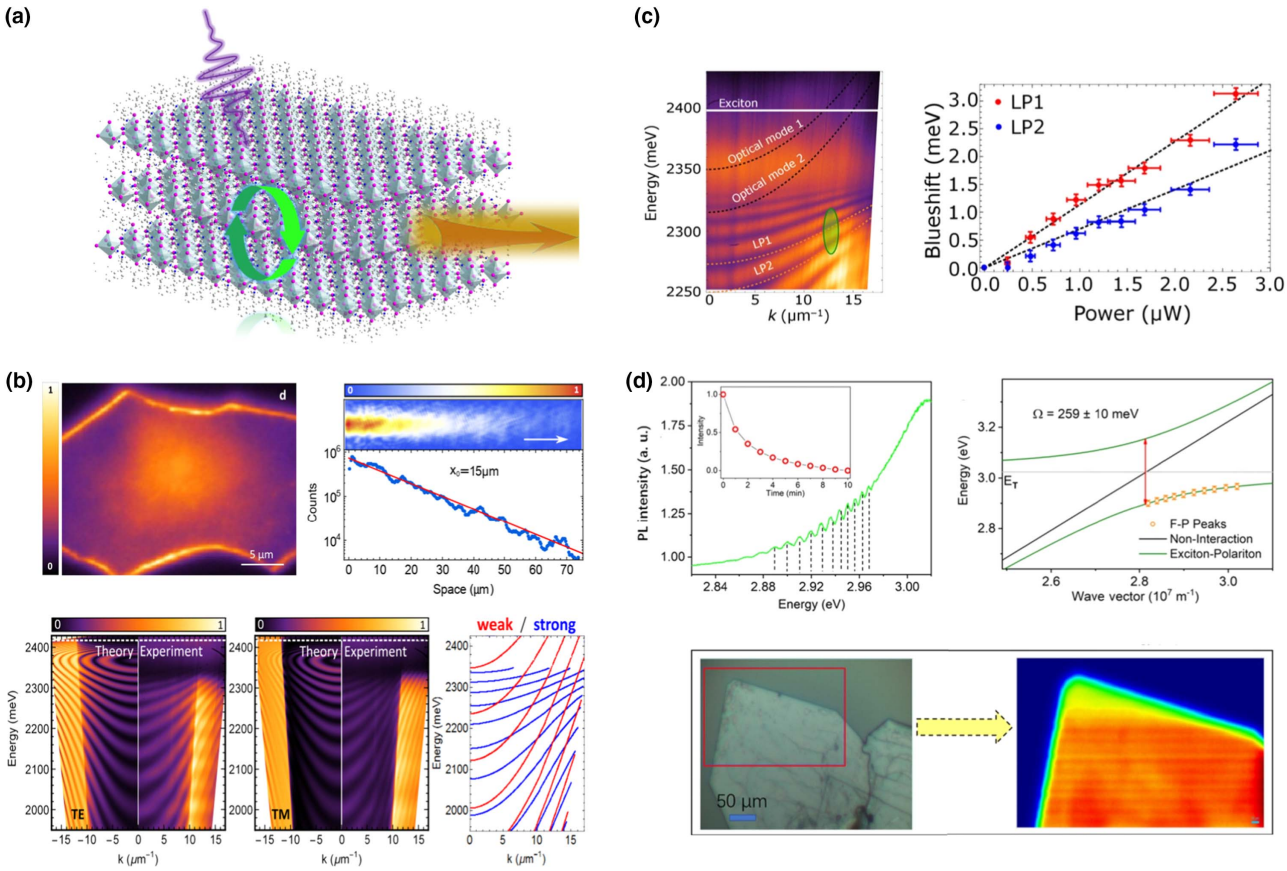

Fig. 5. Polariton in 2D perovskite self-organized crystal cavity. (a) Schematic diagram showing the oscillation of light between top and bottom interface of 2D perovskite single crystal (green arrow) and in-plane transmission of light inside the perovskite crystal (yellow arrow). (b) In-plane and out-of-plane exciton polariton in $(PEAI)_2PbI_4$ crystal. Top left is the PL image of perovskite crystal; right is the real-space intensity image of a resonant injected beam in the perovskite crystal; bottom, energy-momentum resolved reflection spectra of TE (left) and TM (middle) polarizations; the calculated reflection minima with (blue lines) and without (red lines) the interaction of excitonic resonance indicating the strong light-matter coupling. Adapted with permission from [33]. Copyright 2018, American Chemical Society. (c) Energy dispersion of a 2D perovskite $(PEAI)_2PbI_4$ single crystal showing the multimode exciton polaritons. The two low polariton modes (blue region) under different pumping power show energy blueshift of different values, indicating the exciton polariton nonlinearity. Adapted from [102]. Copyright 2019, AAAS. (d) Upper side, PL spectra consisting of a series of oscillating modes in a 2D perovskite planar cavity. The relation of oscillating modes versus wave vector can be fitted by a polariton model with a large Rabi splitting. Bottom is the PL mapping of a selected area of 2D perovskite planar crystal cavity. The interference pattern indicates the oscillating emission of exciton polariton. Adapted with permission from [56]. Copyright 2020, American Chemical Society.

of exciton and F–P mode photon was verified by reflectivity spectra at different incident angles. Two dips with an angle-dependent energy position, linewidth, and intensity were observed with anticrossing behavior—a sign of strong exciton–photon coupling. Two dips at different angles can thus be ascribed to the LPB and UPB of polariton dispersion with Rabi splitting of 140 meV [Fig. 6(a)]. They also found that by changing the thickness of spacer layers or perovskite film, the detuning and Rabi splitting can be precisely controlled [81]. Pradeesh *et al.* investigated the exciton–photon coupling in an all-metal cavity containing two silver mirrors and sandwiched 2D perovskite $(C_6H_9C_2H_4NH_3)_2PbI_4$ [Fig. 6(b)] [101]. Compared with open metal-perovskite–air cavity, this cavity enhances the Rabi splitting from 130 meV to 160 meV due to the greater field confinement. However, these cavities often possess low Q factor—no more than 100, which restrains the study of stimulated polaritonic effects. Han *et al.* improved the Q factor by designing a DBR cavity containing two DBR mirrors and the inserted perovskite $(C_6H_5C_2H_4NH_3)_2PbI_4$ layer [59]. During the fabrication, the top dielectric mirror was migrated in liquid to avoid the degradation of perovskite. The far-field emission map in Fig. 6(c) reveals the dominated emission from middle polariton branches (MPBs); the linewidth of the MPB is 26 meV, corresponding to a Q factor of 86. In recent years, the Q factor of vertical F–P cavities has significantly improved due to the use of DBR cavities coupled with 2D perovskite single crystals, which promotes the observation of new polaritonic effects. Wang *et al.* observed that in a DBR cavity containing 2D perovskite crystal microplates, multimode polariton barchans are not only from the strong coupling of excitons and cavity modes, but also the Bragg modes from the Bragg mirrors [60]. Thus, the reversible energetic exchange can be established in these three states. In DBR cavity of $(PEA)_2PbI_4$, Fieramosca *et al.* found that

the polariton blueshift is sensitive to the polarization of the pump laser. The blueshift obtained with a circularly polarized laser is higher than the blueshift obtained by using a linearly polarized laser. This indicates the existence of different spins of polaritons influencing the polariton–polariton interaction [102]. The spin-dependent nonlinearities can be applied to spintronics, which is only available at cryogenic temperatures for GaAs-based systems [105]. Very recently, Polimeno *et al.* reported the polariton condensation in a vertical cavity containing exfoliated $(PEA)_2PbI_4$ sandwiched between a bottom Bragg mirror and a top silver mirror at liquid helium temperature [106]. This was confirmed by a two-laser threshold behavior under increasing pump fluence. The first laser threshold was assigned to a biexciton lasing action above the bottom of the LPB. Further increasing the pump fluence led to shutdown of the biexciton lasing and the population collapse to the bottom of the LPB as a sign of bosonic condensate. The author thus argued that a simple two-level system is not adapted to such material because of the energetically competitive lasing action. This stimulated polariton phenomenon suggests the exploration of quantum coherent states based on 2D perovskites.

3. Exciton–Polariton in Photonic Crystals of 2D Perovskite

2D perovskite can be effectively coupled with a period lattice structure owing to its solution processing and soft nature, allowing the mismatched growth on different substrates. The first attempt was done by Fujita *et al.* [100]. They fabricated a distributed feedback (DFB) cavity on a quartz substrate and spin-coated a 30 nm thick $(PEA)_2PbI_4$ film followed with a polystyrene film [Fig. 7(a)]. The dispersion of DFB-guided wave-like modes and coupling with excitons were obtained by plotting the transmission dip at different angles. Anticrossing behaviors can be observed at 2.4–2.5 eV with polariton splitting of ~100 meV. The dielectric DFB structure can be further replaced by silver gratings. Niu *et al.* reported the strong coupling of excitons and the surface plasmon polaritons (SPPs) in this kind of structure [Fig. 7(b)] [71]. In this structure,

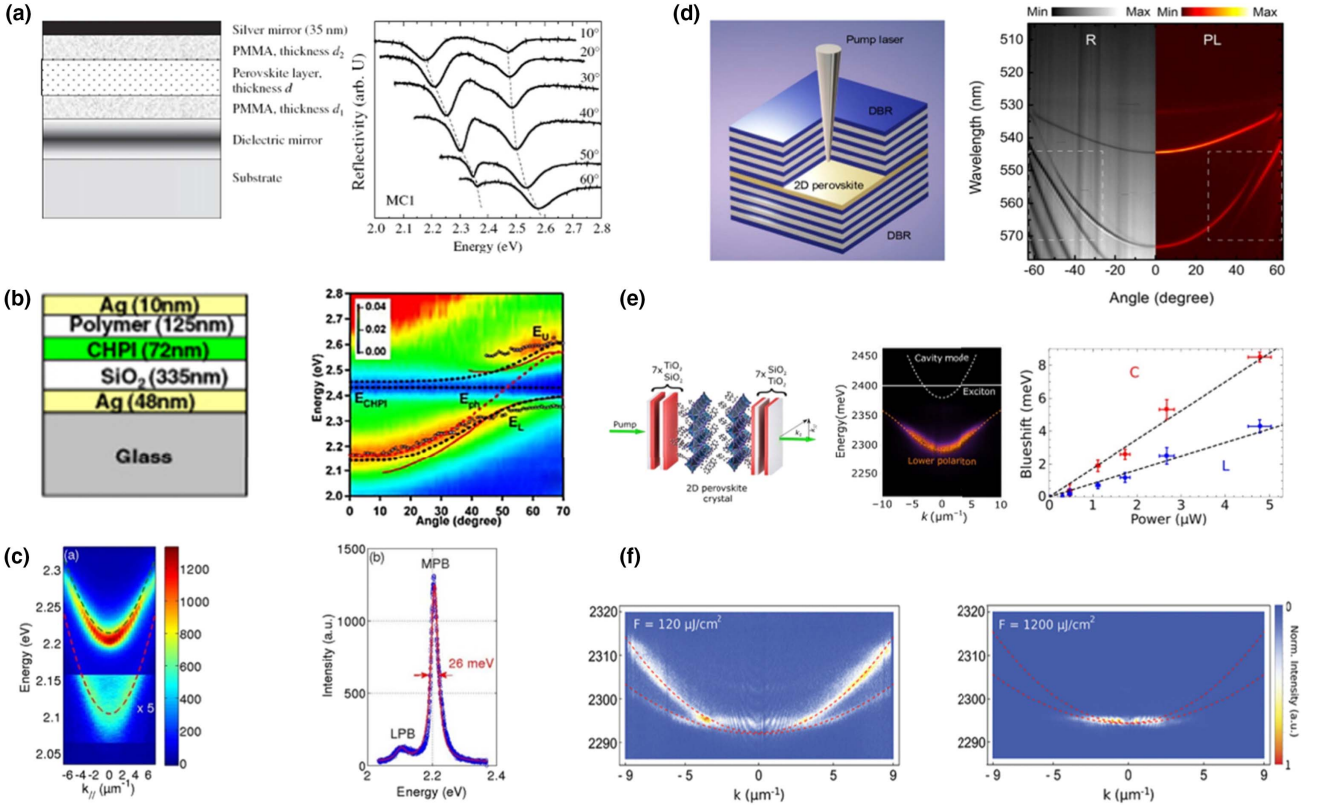

Fig. 6. Polariton in vertical F–P cavities coupled with 2D perovskite. (a) Sketch of a microcavity containing 2D perovksite thin film. Anticrossing is observed in angle-resolved reflectivity spectra as two series of dips. Adapted from [81]. Copyright IOP Publishing and Deutsche Physikalische Gesellschaft. Reproduced by permission of IOP Publishing. All rights reserved. (b) Vertical F–P cavity of 2D perovskite thin flim formed by top and bottom silver films. Two polariton branches can be observed in angle-resolved transmission spectra with Rabi splitting of 160 meV. Adapted with permission from [101]. Copyright The Optical Society. (c) Energy dispersion of micro PL spectrum in a 2D perovskite cavity with relatively high Q factor; the emission of MPB is as narrow as 26 meV. Adapted with permission from [59]. Copyright The Optical Society. (d) Strong coupling of exciton with vertical cavity mode and Bragg modes in a DBR cavity of 2D perovskite. Left, cavity structure consisting of exfoliated 2D perovskite microflakes between top and bottom Bragg mirrors; right, angle-resolved reflection and emission spectra. Adapted with permission from [60]. Copyright 2018, American Chemical Society. (e) Polarization-sensitive polariton nonlinearity of 2D perovskite. Left, cavity structure of a DBR cavity; middle, energy momentum k emission; right, polariton blueshift at different pump powers by using a linearly polarized (L) laser and a circularly polarized (C) laser. Adapted from [102]. Copyright 2019, AAAS. (f) Formation of biexciton laser (left) and polariton condensate (right) in a $(PEA)_2PbI_4$ vertical cavity at liquid helium temperature. Adapted from [106]. Copyright 2020, John Wiley and Sons.

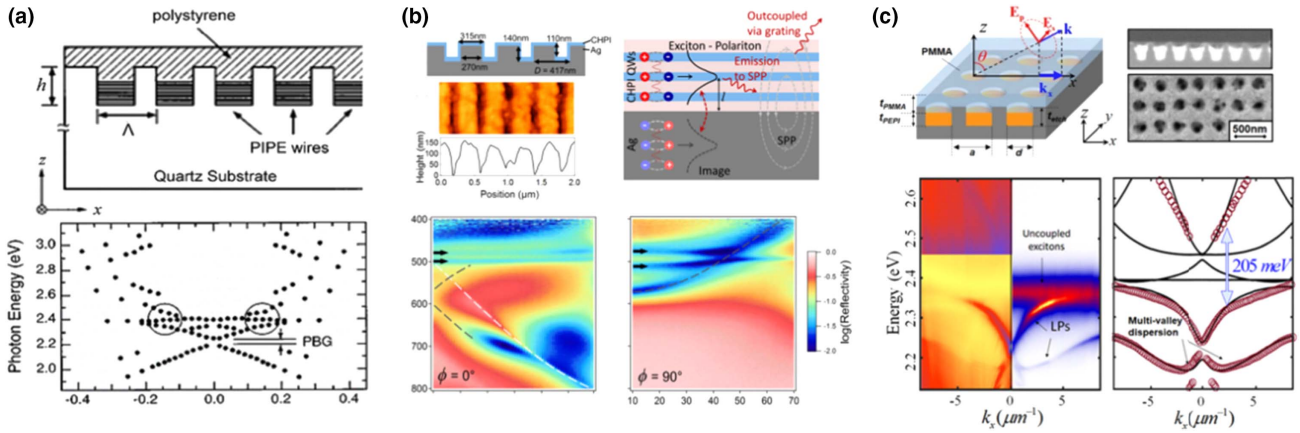

Fig. 7. Polariton in DFB and photonic crystal cavities coupled with 2D perovskite. (a) Structure of a DFB microcavity containing $(PEA)_2PbI_4$ (upper) and energy dispersion of transmission dips indicating the strong coupling of exciton and grating modes. Adapted with permission from [100]. Copyright 1998, American Physical Society. (b) Plasmon-exciton strong coupling in silver grating overcoated with 2D perovskite. Top left, cross section of the grating structure; top right, possible emission routes of SPP-mediated image biexciton; bottom, TM-polarized reflectivity at different incident angles. Adapted with permission from [71]. Copyright 2015, American Physical Society. (c) Exciton polariton of perovskite-based 2D lattice cavity structure: top, cavity design and scanning electron microscope (SEM) images of metasurface; bottom, angle-resolved reflection and emission (left) and corresponding simulation of photonic crystal polariton dispersion (right) with a Rabi splitting of 205 meV. Adapted with permission from [62]. Copyright 2020, American Chemical Society.

an "image biexciton" is formed by the out-of-plane interaction of exciton and the electromagnetic field near the silver surface. By increasing the incident angle from 0° to 90°, the exciton splitting increases, the grating modes become more dispersive, and the plasmonic modes are more resonant with the exciton and image biexciton energy. As a result, strong coupling between SPPs and exciton/image biexciton can be observed with Rabi splitting of 150 and 125 meV, respectively. In addition, a 2D periodic lattice cavity coupled with 2D perovskite was also reported recently [Fig. 7(c)] [62]. The cavity was fabricated through infiltrating $(PEA)_2PbI_4$/DMF solution inside the air hole of a periodically patterned SiO_2 backbone. Angle-resolved reflection and PL spectra reveal the strong coupling between Bloch modes with $(PEA)_2PbI_4$ excitons, along with a Rabi splitting of ~200 meV. Many polariton-dispersive properties such as linearity, slow light, and multivalley polariton mode can also be modified in this 2D lattice cavity.

B. Optical Gain and Photonic Laser of 2D Perovskite Cavity Structures

The generation of lasers requires high optical gain material coupled with a suitable optical cavity. The gain materials that can amplify light through stimulated emission play the important role in laser performance and encourage the discovering of new optical gain materials. Perovskites have shown excellent optical gain coefficients that are comparable to industrial gain materials such as GaAs [10] Room temperature low-threshold and even continuous-wave pumped lasers have been reported abundantly in 3D perovskites of different cavity structures [63,107–110] since the first observation of room temperature amplified spontaneous emission (ASE) in 3D perovskites in 2014 [111]. Comparatively, the ASE of a 2D perovskite was first observed in 1998 without much attention due to the operation at cryogenic temperatures [112]. Although both 3D and 2D perovskites possess some similar photoelectric performance such as efficient LEDs and high photoelectric conversion efficiency (PCE) of solar cells [6,113], the intrinsic differences in crystal and electrical structures are still considerable in photophysical processes such as recombination of photon-excited states.

In 3D perovskites, the exciton binding energy is generally modest, which indicates the coexistence of free carriers and excitons [114]. Based on the Saha–Langmuir equation describing the population distribution of free carriers and excitons [115], the exciton fabrication should be increased at high excitation density. However, this relation becomes invalidated when the carrier density approaches the Mott density, indicating the transition from exciton to free carriers [Fig. 8(a)] [116]. For 3D perovskite with low binding energy, such as $MAPbI_3$, free carriers dominate, even below Mott density, and the origin of lasing can be argued as the electron-hole recombination [117]. The judgment becomes complicated when the threshold density is located near the Mott density where the excitons are not a minority in $CsPbBr_3$ [118,119]. Marongiu *et al.* compared the power law of instantaneous PL intensity versus injected carrier density for 3D perovskite $MAPbI_3$ and 2D perovskite BA_2PbBr_4 under the pulse excitation of a 50 ps window [Fig. 8(b)] [120]. The quadratic behaviors in $MAPbI_3$ indicate bimolecular recombination at an all-density region at room temperature; a linear relation only exists in a low excitation region at cryogenic temperatures. In 2D perovskite with large binding energy, the linear relation in all the excitation ranges suggests the majority of excitons and only a neglectable fraction of ionized excitons, in sharp contrast to 3D perovskite. Indeed, excitonic ASE and lasing of 2D perovskite have been verified in recent years, as is discussed below.

1. Optical Gain in 2D Perovskite

Room temperature optical gain was first observed in 2D perovskite $(NMA)_2(FA)_{n-1}PbnX_{3n+1}$ ($NMA = C_{10}H_7CH_2NH_3^+$)

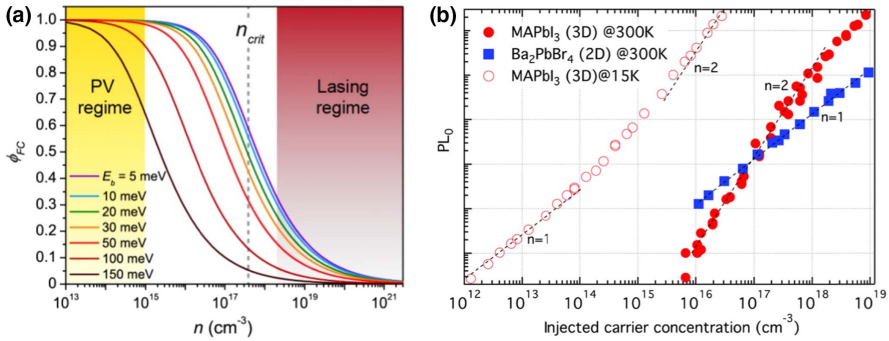

Fig. 8. Excitonic and free-carrier recombination of 2D and 3D perovskites. (a) The fabrication of free carriers over the total excitation density at different binding energies by using the Saha–Langmuir equation. Adapted with permission from [116]. Copyright 2016, American Chemical Society. Further permissions related to the material excerpted should be directed to the ACS. (b) The relation of emission intensity and injected carrier concentration of 3D perovskite $MAPbI_3$ and 2D perovskite BA_2PbBr_4 at different temperatures. The slope indicates dominant bimolecular recombination ($n = 2$) or excitonic recombination ($n = 1$). Adapted from [120] with permission from the Royal Society of Chemistry.

by Li *et al.* [121]. During the formation of 2D perovskite thin film, multiple QW phases of different n values were arranged vertically to substrate from small to large n. These self-organized QWs naturally form an energy cascade, allowing the ultrafast exciton transfer from small n values to large n values with decreasing bandgap [Fig. 9(a)]. ASE was observed by pumping the perovskite thin film with a rectangle strip of femtosecond laser. Below the threshold, emission from large n values ($n > 5$) follows a power law of ~0.86, which is close to 1, indicating the excitonic recombination of spontaneous emission. When above the threshold, a sharp peak arises from the red side of the spontaneous emission (SE) peak. The optical gain value of $(NMA)_2FAPb_2Br_7$ can reach 330 cm^{-1}, which is much larger than that of 3D perovskite film with a similar thickness [111,122]. Moreover, the ASE peak can be shifted from 530 to 810 nm by changing the stoichiometry, and the ASE stability at ambient conditions also shows better performance than 3D perovskite thin films [Fig. 9(b)]. In contrast, 2D perovskites with small n values still have difficulty in obtaining room temperature ASE and lasing. Chong *et al.* developed a theoretical model of charge carrier relaxation in $n = 1$ perovskite $(PEA)_2PbI_4$ and explained the limitation of optical gain in this 2D perovskite [123]. The modeling consists of the interaction of free exciton, bound exciton, and bound biexciton in Fig. 9(c). The free exciton trapping and formation of bound exciton can

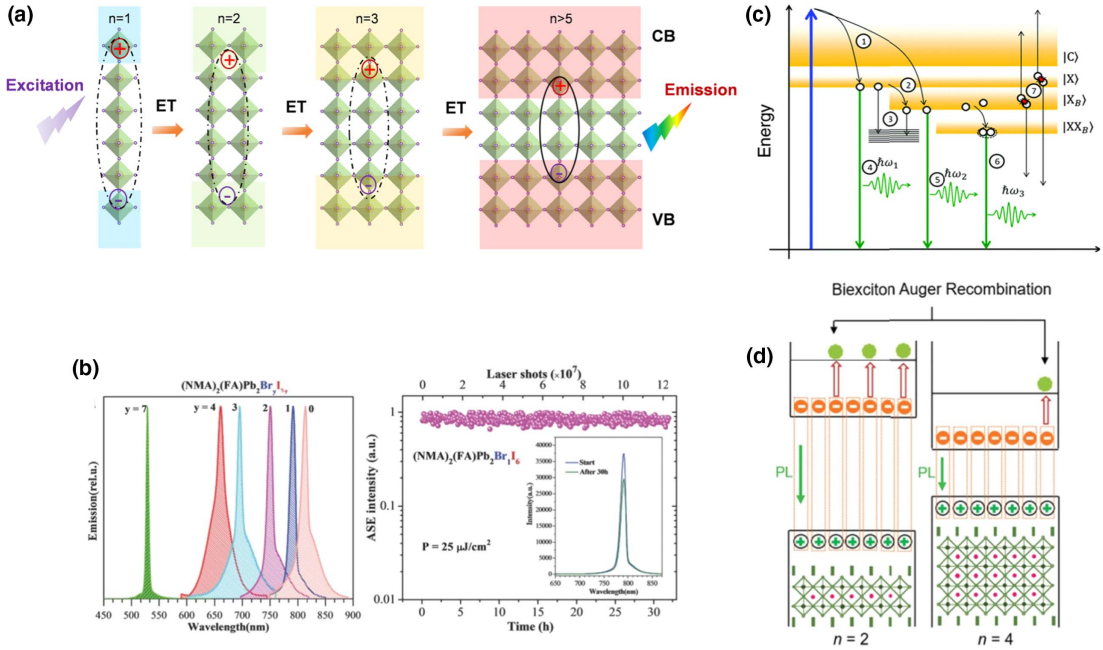

Fig. 9. Optical gain in 2D perovskites. (a) Cascade energy transfer from wide-bandgap QWs to large QWs with increasing n-value; (b) wavelength tunability of 2D perovskite with different y values by mixing precursor solutions and the stability of ASE over 30 h. The inset shows the ASE spectra at the start and after 30 h. Adapted with permission from [121]. Copyright 2018, John Wiley and Sons. (c) Proposed relaxation channels of excitons in $(PEA)_2PbI_4$. Adapted from [123]. Published by the PCCP Owner Societies. (d) Schematic shows the biexciton Auger recombination in 2D perovskites with n values of 2 and 4. Auger recombination becomes stronger at small n values as a result of narrow well and larger spatial confinement of exciton. Adapted with permission from [18]. Copyright 2019, John Wiley and Sons.

effectively compete with biexciton gain, leading to a large biexciton ASE threshold beyond the damage threshold of these materials. Liang *et al.* systemically investigated the PL decay and temperature-dependent PL of pure phase (n value) of $(BA)_2(MA)_{n-1}Pb_nI_{3n+1}$ ($n = 2$–5) and attributed the large laser threshold of small n value 2D perovskites to fast Auger recombination and large exciton-LO phonon coupling in these materials [Fig. 9(d)] [18]. Nonradioactive recombination of these processes restrains the optical gain, which is more obvious at small n values with increased quantum confinement and lattice deformation.

2. Lasing in Self-Assembled 2D Perovskite Crystal Cavities

Li *et al.* demonstrated the room temperature microlaser in solution-processed 2D perovskite $(OA)_2(MA)_{n-1}Pb_nBr_{3n+1}$ (OA = octylamine) with mixed layers of different n values [124]. Multimode WGM laser can be obtained by pumping a single microplate above the threshold of 8.5 $\mu J/cm^2$, which is lower than the ASE threshold of 3D perovskite $MAPbBr_3$ film with a similar thickness. Dual-wavelength lasing can be observed in a single microplate with higher content of low-dimensional layers [Fig. 10(a), top], and no lasing is observed in microplates with pure low-dimensional 2D perovskite ($n = 5$). Micro-area transient absorption (TA) spectroscopy reveals the fast exciton localization from the lower to higher dimensional perovskite layers within 1 ps, which is much shorter than the lasing lifetime. Therefore, efficient exciton localization contributes to the low-threshold lasing [125]. In addition, lasing from these 2D perovskite microplates shows linearly polarized emission [Fig. 10(a), bottom], indicating the photon confinement of higher-dimensional perovskite layers given by the cladding layers of lower-dimensional perovskite layers (small refractive index). However, high-quality homologous 2D perovskite single crystals are still essential for the deep understanding of the fundamental physical properties. Raghavan *et al.* observed the room temperature low-threshold lasing from $(BA)_2(MA)_{n-1}Pb_nI_{3n+1}$ homologous single crystal with different n (1, 2, and 3) in Fig. 10(b) [57]. Laser modes consist of several small spikes around a few strong sharp peaks, which can be proposed as random lasing or light-trapping inside the crystals [126,127]. Since 2D perovskite can be exfoliated from the bulk crystals, Liang *et al.* investigated the lasing behaviors of $(BA)_2(MA)_{n-1}Pb_nI_{3n+1}$ thin flakes with thicknesses of 100–300 nm in Fig. 10(c) [18]. For the microflakes of $n = 3$ perovskite, lasing can occur at pump fluence of 2.6 $\mu J/cm^2$ and temperature of 78 K. Since the shapes of microflakes are not well defined, light can leak out from the edge of the in-plane cavity. However, no stimulated emission was obtained in $n = 1$, 2 microflakes, even at a low temperature of 78 K, which is different from the lasing in bulk crystals. At higher temperatures, the laser threshold dramatically increases as a result of increased electron–phonon scattering. The steeper increase of threshold at small n values indicates the weak thermal stability and large optical losses in low-dimensional perovskite layers.

3. Lasing in 2D Perovskite Cavity Arrays

Integrated laser arrays can be applied in full color display and sensing applications [128]. 2D perovskites hold great advantages for laser array engineering, considering the ease of integration to different cavity structures and for high optical gain. Zhang *et al.* demonstrated 2D perovskite laser arrays composed of microrings and nanowires by the structure-templated methods [61,77]. The desired $(BA)_2(MA)_{n-1}Pb_nBr_{3n+1}$ cavity with nominal value of 2 actually consists of QWs with $n \geq 2$ to ∞, resulting in different exciton energy values [Fig. 11(a)]. As discussed above, such energy cascades can result in efficient energy transfer between QWs from small n values to large n values. ASE measurement on 2D perovskite film showed that no ASE was obtained at small n values 1–3, and $n = 6$ perovskite thin film exhibited the best ASE performance with low threshold and high gain [Fig. 11(b)]. Consequently, they selected the $n = 6$ 2D perovskite as the gain medium of microring laser arrays. Upon the pumping by a 400 nm pulsed laser, microring cavity arrays generated laser modes around 543 nm with a high Q factor of 2600. Similarly, nanowire laser arrays

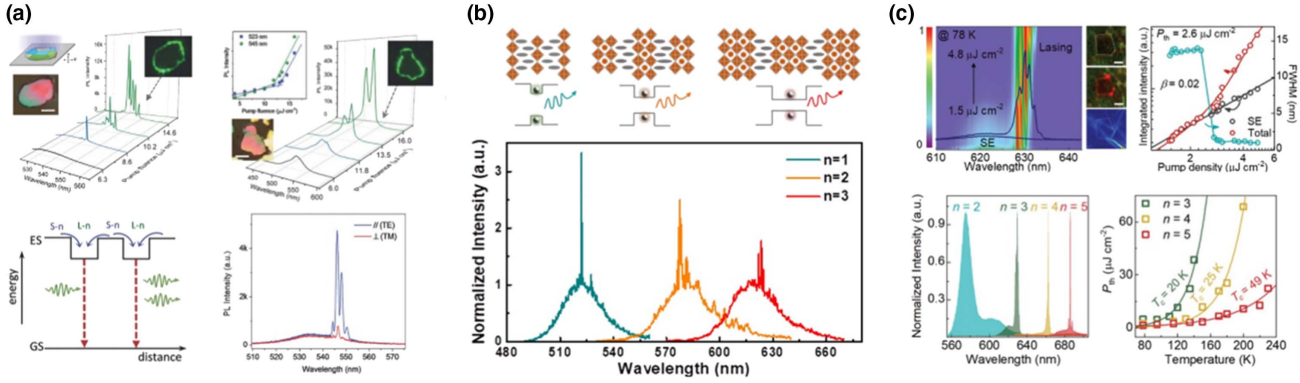

Fig. 10. Lasing behaviors of 2D perovskite self-organized crystal cavity. (a) Top, lasing of a single 2D perovskite microplate (left) and dual-wavelength lasing (right) from 2D perovskite with $n = 6$ and $n \geq 7$. The insets show the corresponding optical images, PL images above laser threshold, and PL intensity as a function of pump fluence. Adapted with permission from [124]. Copyright 2018, John Wiley and Sons. (b) Lasing spectra from homologous 2D perovskite single crystals with different n values and bandgaps. Adapted with permission from [57]. Copyright 2018, American Chemical Society. (c) Lasing of exfoliated 2D perovskite microflakes. Top, lasing spectra (left) and integrated intensity (right) of $n = 3$ under different pump fluences and corresponding optical images; bottom, lasing (n = 3–5) and ASE ($n = 2$) spectra of 2D perovskite with different n values and corresponding lasing thresholds at different temperatures. Adapted with permission from [18]. Copyright 2019, John Wiley and Sons.

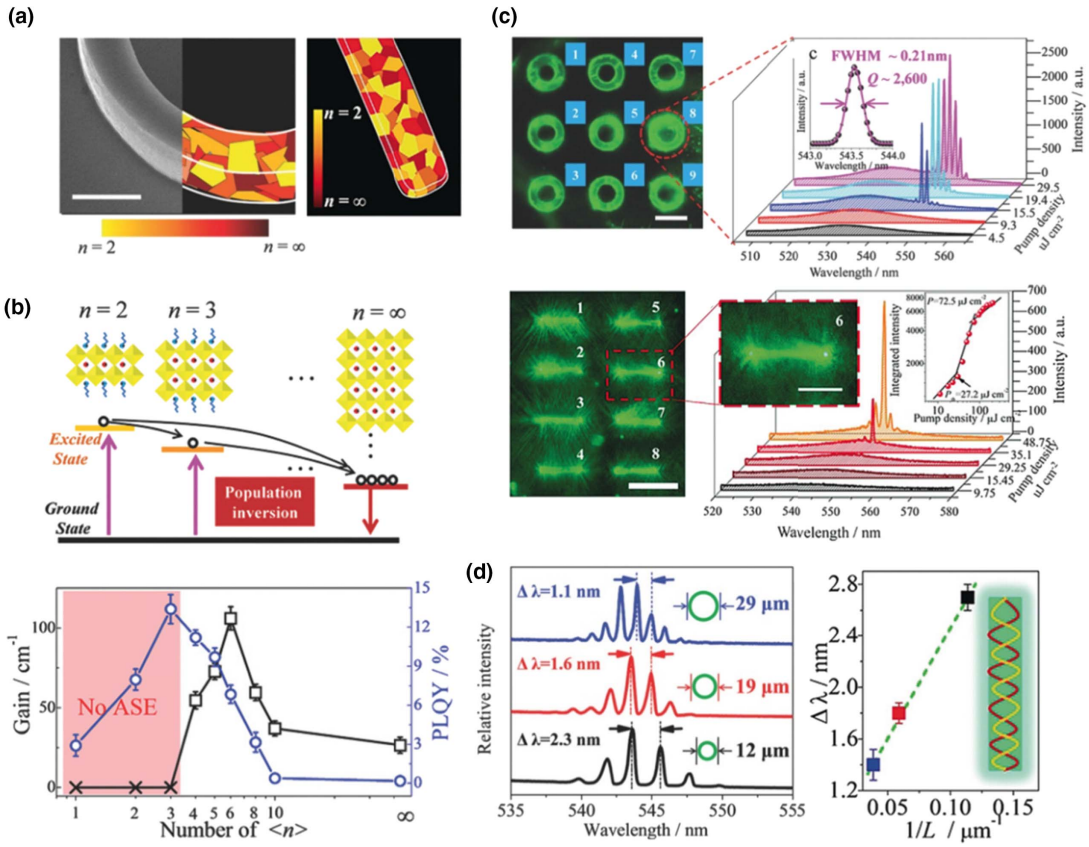

Fig. 11. Lasing behaviors of 2D perovskite microcavity array. (a) SEM image and schematics show the microring and nanowire structures consisiting of multi-QW structure; (b) top, light harvesting of the nominal $n = 2$ perovskite thin film for ASE; bottom, gain coefficient and PLQY for perovskite thin film with different nominal n values; (c) emission images and lasing spectra of microring (upper) and nanowire (lower) arrays at different pump fluences; (d) relation of lasing mode spacing versus ring diameter or nanowire length indicating the WGM lasing mode of microring array (left) and F–P lasing mode of nanowire array (right). Adapted with permission from [61,77]. Copyright 2018, John Wiley and Sons.

were also fabricated, and a multimode laser was obtained around 548 nm with a laser threshold of 72.5 μJ/cm^2 [Fig. 11(c)]. The oscillating type of microring and nanowire arrays were confirmed as WGM mode and F–P mode by comparing the mode spacing of adjacent laser modes versus the cavity length of different sizes of microrings and nanowires, respectively [Fig. 11(d)] [129,130].

4. Lasing in 2D Perovskite-Embedded Vertical F–P Cavities

Vertical cavity structures consisting of Bragg mirrors and/or metallic reflectors are essential for the fabrication of VCSELs with a high Q factor and a reduced threshold [131]. A room-temperature VCSEL of a quasi-2D perovskite $(PEA)_2Cs_{n-1}Pb_nBr_{3n+1}$ is obtained in a vertical cavity embedded with the microcrystals of the quasi-2D perovskite [Fig. 12(a)] [17]. The active layer is designed as a sandwich structure of perovskite/PMMA/perovskite, resulting in the self-organized segregated patterns and surrounding thinner smooth film of quasi-2D perovskite with diverse phases (n values). Interestingly, lasing can only be observed in segregated areas under the nanosecond pulsed laser, which might benefit from the reduction of the surface trap by long-chain PEA and energy transfer within the crystal [121]. A single-mode laser occurred at 532 nm, which slightly blueshifts to the cavity mode at 534 nm. The lasing threshold of ~500 μJ/cm^2 is the same order of VCSEL in $CsPbBr_3$ QDs and 3D perovskite film pumped by a nanosecond laser [132,133], which suggests the possibility of continuous-wave pumped laser of 2D perovskite. In the vertical cavity of another 2D perovskite $(DA)_2PbI_4$ (DA = dodecylammonium), biexciton lasing is even observed at an intermediate temperature up to 125 K [Fig. 12(b)] [134], which is much higher than the biexciton lasing of 2D perovskite $(HA)_2PbI_4$ [112] at 16 K. The cavity is fabricated by spin-coating 25 nm of DA_2PbI_4 and a spacer layer of PMMA between a Bragg mirror and a silver layer. Biexcitons of DA_2PbI_4 were found to have a large binding energy of 50 meV, which was ready for the operation of biexciton lasing at high temperature. Lasing occurs from the low-energy tail of biexciton emission spectra and supports the narrowing peak and the s-like curve of emission intensity at different pump fluence. Room temperature laser in this material can be expected with improved fabrication of cavity structure and material source.

C. Functional Devices of 2D Perovskite Photonic Structures

Optical cavities can enhance the emission or absorption and modulate the guided optical modes in a desired energy region.

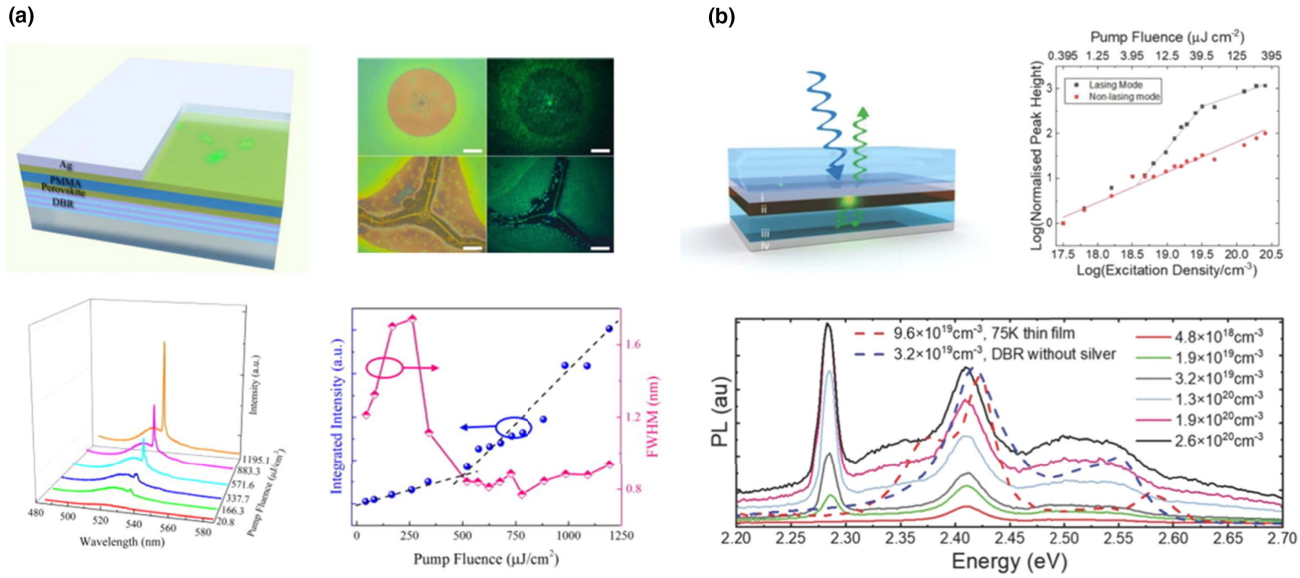

Fig. 12. Lasing behaviors of 2D perovskite embedded vertical F–P cavity. (a) Lasing of segregated quasi-2D perovskite microcrystals in vertical cavity: top, schematic of cavity structure (left) and PL images (right) of segregated patterns; bottom, pump fluence-dependent emission spectra, integrated intensity, and FWHM, indicating the lasing threshold of ~500 μJ/cm^2. Adapted from [17] with permission of AIP Publishing. (b) Vertical cavity biexciton lasing of 2D perovskite: top left, schematic of DBR cavity consisting of Bragg mirror, spin-coated DA_2PbI_4, PMMA, and top silver mirror; top right, pump fluence-dependent cavity emission at 2.28 and 2.41 eV, indicating the lasing mode and nonlasing mode; bottom, emission spectra of cavity at different optical pump powers with and without silver mirror, and perovskite thin film on glass. Adapted from [134]. Copyright 2018, John Wiley and Sons.

The cooperation of photonic structures and optoelectronic devices is expected to enhance the device performance and/or realize new device functions [90,135].

Liu *et al.* developed a perovskite-microsphere hybrid structure to enhance the two-photon absorption-induced PL (TPL) of 2D perovskite $(PEA)_2PbI_4$ [136]. This was done by transferring the SiO_2 microspheres onto a perovskite flake under a microscope. Under the pumping of pulsed laser of 800 nm (8 fs, 80 MHz), TPL from the perovskite flake exhibited a small green spot with a modest emission intensity. In contrast, TPL from the perovskite-microsphere structure was much stronger and appeared as a large "bright ball" [Fig. 13(a)]. TPL spectra revealed the enhanced TPL by 2 orders of magnitude from the perovskite-microsphere structure [Fig. 13(b)], which can be explained as a nanofocusing enhanced optical field [137] and improved TPL detection efficiency [138] by the sphere cavity. Field-enhanced operation can also be obtained by plasmonic effects or photonic crystals, which have been reported in 3D perovskite-based solar cells and photodetectors [139–142].

2D perovskite nanowires with optical anisotropy have also been adopted in efficient light detection devices. Feng *et al.* fabricated a photodetector consisting of 2D perovskite nanowire arrays between two silver electrodes [Fig. 14(a)] [143]. Unlike polycrystalline film with many surface defects and grain boundaries, single-crystalline nanowires with pure (101) crystallographic orientation allow the efficient excitons to diffuse to the edge along the short length side and dissociate into free carriers through exciton edge states [144]. In addition, efficient charge transport in well layers and photocarriers concentration at the surface of layer edges result in a high photoconductivity channel at the layer edges. The detector exhibits high average responsivities of 1.5×10^4 A/W and detectivities over 7×10^{15} Jones with suppressing dark currents. Later, Ghoshal *et al.* observed the highly polarized PL from 2D perovskite $(BA)_2PbI_4$ nanowires and further the anisotropic photocurrent [Fig. 14(b)] [53]. PL emission is boosted when the polarization of excited light is parallel to the length of nanowire and weakened when it is perpendicular to the nanowire. The polarization ratio increases up to 0.73 with reduced lateral width as a result of dielectric confinements. Further, polarized photodetection is demonstrated, consisting of a graphene/$(BA)_2PbI_4$ nanowire heterostructure. The bump at 518 nm is consistent with the excitonic absorption, indicating the photocurrent response from the optical behaviors of the perovskite nanowire.

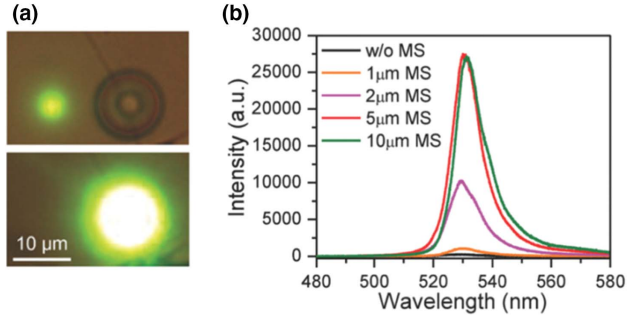

Fig. 13. Enhanced TPL emission from a 2D perovskite-microsphere cavity structure. (a) Emission images of pure perovskite flake and with SiO_2 microsphere under the pump power of 0.1 mW; (b) TPL spectra of bare perovskite flake and perovskite-microsphere cavity structures with different sizes of microspheres. Adapted with permission from [136]. Copyright 2018, John Wiley and Sons.

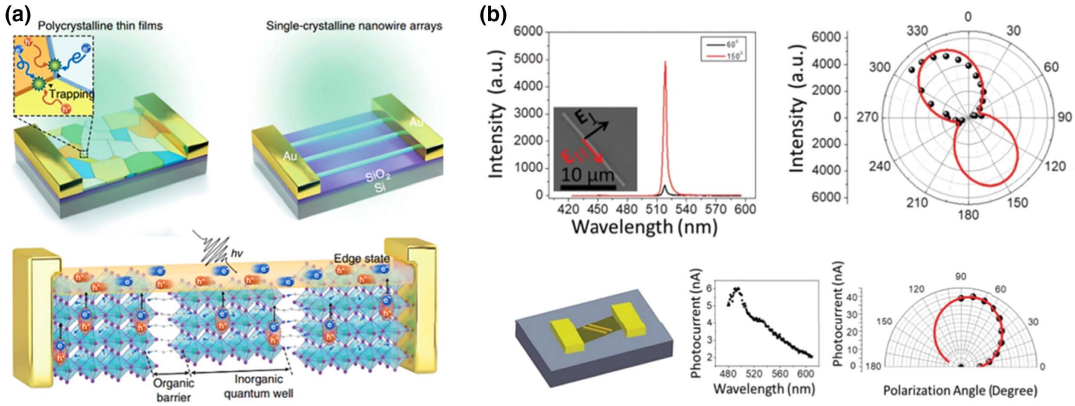

Fig. 14. Ultrasensitive and polarized light detection of 2D perovskite nanowires. (a) Schematics of 2D perovskite nanowire photodetectors. Top, photodetectors based on polycrystalline thin films and nanowire array; bottom, carrier dynamics in the photodetector of single crystalline nanowires indicating the organic barriers for suppressing the dark current and conductive channels at crystalline edges for excitonic dissociation and free-carrier conduction. Adapted from [143] with permission of Springer Nature, Nature Electronics, Copyright 2018. (b) 2D perovskite nanowires for polarized light detection: top, PL spectra excited by light with polarization parallel (red) and perpendicular (black) to the nanowire orientation (left) and polar plot of PL intensity with different excitation polarizations (right); bottom, schematic of the perovskite/graphene hybrid device (left), photocurrent as a function of excitation energy at fixed power and source-drain voltage (middle), and polarization dependent photocurrent under pulsed laser at 2.52 eV and source-drain bias of 30 mV (right). Adapted with permission from [53]. Copyright 2019, John Wiley and Sons.

Polarized light detection can be observed, as the photocurrent is strongly dependent on the angle between the polarization of incident light and the orientation of nanowires, which is similar to the polarized PL spectra. Apart from photodetection, nanowires can also be applied in optical logical gates, waveguides, etc. [145–147], which need further exploration in 2D perovskites.

5. SUMMARY AND OUTLOOK

2D perovskites have become attractive active materials for photonic applications over the past few years. The advantages of these materials lies in the quantum-well-like structures sustaining strong excitonic emission with large binding energy, and ease of integration with different kinds of optical cavities. The review summarizes the recent advances in the cavity application of 2D perovskites, as well as the inherent photophysics and light-matter interaction in the cavity structures of 2D perovskites. The accelerating investigations in 2D perovskite-based photonics reveal fantastic structure-related optoelectronics that are different from their 3D counterparts and conventional layered semiconductors to some degree. Moreover, the flexibility of organic ligands, halide ions, and dimensionality highly expands their optoelectronic behaviors. New types of photonic devices can thus be expected in 2D perovskite-based photonic structures. We should also note that there are still many issues concerning the practical usage and production of 2D perovskite-based photonics that need further investigation.

Different synthetic methods have been explored for 2D perovskites. The most convenient and productive way is spin-coating the as-prepared solution to form 2D perovskite thin film on different structures. However, the intrinsic surface traps and grain boundaries of thin film are drawbacks for efficient device performance. Single-crystal form 2D perovskite-based photonic structures usually behave with better cavity Q factor and radiative efficiency. Antisolvent methods have shown advantages in fabrication of large-area single-crystalline bulk film, which are still time-consuming and uncontrollable in shape and limited by the substrates. Vapor-phase syntheses by CVD are relatively few, partly due to the complexity of organic components and the uncontrollability of gas flow, which are sensitive factors for different phases of 2D perovskites. Large-scale growth of 2D perovskite single-crystalline film with controlled thickness on desired substrates and structures still calls for further exploration.

Strong exciton–photon coupling and lasing behaviors of 2D perovskite-based cavities, which are still not yet clearly understood, are highlighted in the review. In 2D perovskite with low quantum-well thickness, i.e., n value, photon-induced excitons are believed to be a dominating factor, and lasing machines are considered as excitonic optical gains. However, with increasing n value and a trend to a more 3D-like perovskite, the evolution of lasing machines needs further investigation, considering the increasing fabrication of free carriers and possible optical dipoles between different inorganic layers. In addition, strong exciton–photon coupling of 2D perovskites is robust, with large Rabi splitting energy; however, so far, stimulated polariton behavior is only found in $n = 1$ type of 2D perovskites at cryogenic temperatures. Compared to 3D perovskites, charge carriers' dynamics of 2D perovskites are found to be rather intricate, such as the formation of edge states in the interface of perovskites [144] and excitonic transport [14] between different layer numbers. The interplay of excitonic dynamics and optical oscillation of photonic cavities are thus unique in various kinds of 2D perovskites. Hence, the dynamics of laser generation and the formation of polariton on different 2D perovskite active materials should be investigated in order to give better understanding of the light-matter interaction and pave the way for practical coherent photonic and polaritonic applications.

Functional devices can be expected in the integration of 2D perovskites with photonic cavities. For example, the observed nonlinear optics in 2D perovskites such as second harmonic generation (SHG) and TPL [26], and chiral photonics of 2D perovskites by introducing chiral organic ligands [148] can be amplified and/or guided by the coupled photonic cavities. Cavity enhancement or modification of these effects provides enormous potential in obtaining lower-power and highly sensitive optoelectrical devices. The limitations of 2D perovskites for practical functional devices are their potential toxicity and low stability under ambient environments, although they are believed to be more tolerant than 3D perovskites. We believe that these problems can be relieved in future works with developed tactics including lead-free perovskite and encapsulating technology.

Funding. Strategic Priority Research Program of the Chinese Academy of Sciences (XDB36000000); Ministry of Science and Technology (2016YFA0200700, 2017YFA0205004); National Natural Science Foundation of China (21673054, 11874130); Open Research Fund Program of the State Key Laboratory of Low-Dimensional Quantum Physics (KF201902).

Disclosures. The authors declare no conflicts of interest.

REFERENCES

1. E. M. Purcell, "Spontaneous emission probabilities at radio frequencies," in *Confined Electrons and Photons* (Springer, 1995), p. 839.
2. K. Lagoudakis, *The Physics of Exciton-Polariton Condensates* (PPUR Polytechniques, 2013).
3. D. Sanvitto and S. Kéna-Cohen, "The road towards polaritonic devices," Nat. Mater. **15**, 1061–1073 (2016).
4. Z. Li, T. R. Klein, D. H. Kim, M. Yang, J. J. Berry, M. F. A. M. van Hest, and K. Zhu, "Scalable fabrication of perovskite solar cells," Nat. Rev. Mater. **3**, 18017 (2018).
5. H. Wang and D. H. Kim, "Perovskite-based photodetectors: materials and devices," Chem. Soc. Rev. **46**, 5204–5236 (2017).
6. L. N. Quan, B. P. Rand, R. H. Friend, S. G. Mhaisalkar, T.-W. Lee, and E. H. Sargent, "Perovskites for next-generation optical sources," Chem. Rev. **119**, 7444–7477 (2019).
7. M. A. Green, A. Ho-Baillie, and H. J. Snaith, "The emergence of perovskite solar cells," Nat. Photonics **8**, 506–514 (2014).
8. Q. Dong, Y. Fang, Y. Shao, P. Mulligan, J. Qiu, L. Cao, and J. Huang, "Electron-hole diffusion lengths> 175 μm in solution-grown $CH_3NH_3PbI_3$ single crystals," Science **347**, 967–970 (2015).
9. K. X. Steirer, P. Schulz, G. Teeter, V. Stevanovic, M. Yang, K. Zhu, and J. J. Berry, "Defect tolerance in methylammonium lead triiodide perovskite," ACS Energy Lett. **1**, 360–366 (2016).
10. B. R. Sutherland and E. H. Sargent, "Perovskite photonic sources," Nat. Photonics **10**, 295–302 (2016).
11. D. H. Cao, C. C. Stoumpos, O. K. Farha, J. T. Hupp, and M. G. Kanatzidis, "2D homologous perovskites as light-absorbing materials for solar cell applications," J. Am. Chem. Soc. **137**, 7843–7850 (2015).
12. C. M. M. Soe, G. P. Nagabhushana, R. Shivaramaiah, H. Tsai, W. Nie, J.-C. Blancon, F. Melkonyan, D. H. Cao, B. Traoré, L. Pedesseau, M. Kepenekian, C. Katan, J. Even, T. J. Marks, A. Navrotsky, A. D. Mohite, C. C. Stoumpos, and M. G. Kanatzidis, "Structural and thermodynamic limits of layer thickness in 2D halide perovskites," Proc. Natl. Acad. Sci. USA **116**, 58–66 (2019).
13. J. C. Blancon, A. V. Stier, H. Tsai, W. Nie, C. C. Stoumpos, B. Traoré, L. Pedesseau, M. Kepenekian, F. Katsutani, G. T. Noe, J. Kono, S. Tretiak, S. A. Crooker, C. Katan, M. G. Kanatzidis, J. J. Crochet, J. Even, and A. D. Mohite, "Scaling law for excitons in 2D perovskite quantum wells," Nat. Commun. **9**, 2254 (2018).
14. S. Deng, E. Shi, L. Yuan, L. Jin, L. Dou, and L. Huang, "Long-range exciton transport and slow annihilation in two-dimensional hybrid perovskites," Nat. Commun. **11**, 664 (2020).
15. Q. Ou, X. Bao, Y. Zhang, H. Shao, G. Xing, X. Li, L. Shao, and Q. Bao, "Band structure engineering in metal halide perovskite nanostructures for optoelectronic applications," Nano Mater. Sci. **1**, 268–287 (2019).
16. V. Ardizzone, L. De Marco, M. De Giorgi, L. Dominici, D. Ballarini, and D. Sanvitto, "Emerging 2D materials for room-temperature polaritonics," Nanophotonics **8**, 1547–1558 (2019).
17. W. Zhai, C. Tian, K. Yuan, C. Ge, S. Zhao, H. Yu, Y. Li, W. Chen, and G. Ran, "Optically pumped lasing of segregated quasi-2D perovskite microcrystals in vertical microcavity at room temperature," Appl. Phys. Lett. **114**, 131107 (2019).
18. Y. Liang, Q. Shang, Q. Wei, L. Zhao, Z. Liu, J. Shi, Y. Zhong, J. Chen, Y. Gao, and M. Li, "Lasing from mechanically exfoliated 2D homologous Ruddlesden-Popper perovskite engineered by inorganic layer thickness," Adv. Mater. **31**, 1903030 (2019).
19. C. Lan, Z. Zhou, R. Wei, and J. C. Ho, "Two-dimensional perovskite materials: from synthesis to energy-related applications," Mater. Today Energy **11**, 61–82 (2019).
20. S. Roy, A. S. Sharbirin, Y. Lee, W. B. Kim, T. S. Kim, K. Cho, K. Kang, H. S. Jung, and J. Kim, "Measurement of quantum yields of monolayer TMDs using dye-dispersed PMMA thin films," Nanomaterials **10**, 1032 (2020).
21. X. Gao, X. Zhang, W. Yin, H. Wang, Y. Hu, Q. Zhang, Z. Shi, V. L. Colvin, W. W. Yu, and Y. Zhang, "Ruddlesden-Popper perovskites: synthesis and optical properties for optoelectronic applications," Adv. Sci. **6**, 1900941 (2019).
22. Y.-H. Chang, J.-C. Lin, Y.-C. Chen, T.-R. Kuo, and D.-Y. Wang, "Facile synthesis of two-dimensional Ruddlesden-Popper perovskite quantum dots with fine-tunable optical properties," Nanoscale Res. Lett. **13**, 247 (2018).
23. M. Yuan, L. N. Quan, R. Comin, G. Walters, R. Sabatini, O. Voznyy, S. Hoogland, Y. Zhao, E. M. Beauregard, P. Kanjanaboos, Z. Lu, D. H. Kim, and E. H. Sargent, "Perovskite energy funnels for efficient light-emitting diodes," Nat. Nanotechnol. **11**, 872–877 (2016).
24. Y. Zheng, T. Niu, X. Ran, J. Qiu, B. Li, Y. Xia, Y. Chen, and W. Huang, "Unique characteristics of 2D Ruddlesden-Popper (2DRP) perovskite for future photovoltaic application," J. Mater. Chem. A **7**, 13860–13872 (2019).
25. H. Li, T. Luo, S. Zhang, Z. Sun, X. He, W. Zhang, and H. Chang, "Two-dimensional metal-halide perovskite-based optoelectronics: synthesis, structure, properties and applications," Energy Environ. Mater. (2020).
26. X. Han, Y. Zheng, S. Chai, S. Chen, and J. Xu, "2D organic-inorganic hybrid perovskite materials for nonlinear optics," Nanophotonics **9**, 38 (2020).
27. J. Yan, W. Qiu, G. Wu, P. Heremans, and H. Chen, "Recent progress in 2D/quasi-2D layered metal halide perovskites for solar cells," J. Mater. Chem. A **6**, 11063–11077 (2018).
28. D. Ramirez, J. I. Uribe, L. Francaviglia, P. Romero-Gomez, A. F. I. Morral, and F. Jaramillo, "Photophysics behind highly luminescent two-dimensional hybrid perovskite $(CH_3(CH_2)2NH_3)_2(CH_3NH_3)_2Pb_3Br_{10}$ thin films," J. Mater. Chem. C **6**, 6216–6221 (2018).
29. T. Schmidt, K. Lischka, and W. Zulehner, "Excitation-power dependence of the near-band-edge photoluminescence of semiconductors," Phys. Rev. B **45**, 8989–8994 (1992).
30. H. He, Q. Yu, H. Li, J. Li, J. Si, Y. Jin, N. Wang, J. Wang, J. He, and X. Wang, "Exciton localization in solution-processed organolead trihalide perovskites," Nat. Commun. **7**, 10896 (2016).
31. M.-G. La-Placa, G. Longo, A. Babaei, L. Martínez-Sarti, M. Sessolo, and H. J. Bolink, "Photoluminescence quantum yield exceeding 80% in low dimensional perovskite thin-films via passivation control," Chem. Commun. **53**, 8707–8710 (2017).
32. W. Shen, C. Hu, J. Tao, J. Liu, S. Fan, Y. Wei, C. An, J. Chen, S. Wu, Y. Li, J. Liu, D. Zhang, L. Sun, and X. Hu, "Resolving the optical anisotropy of low-symmetry 2D materials," Nanoscale **10**, 8329–8337 (2018).

33. A. Fieramosca, L. De Marco, M. Passoni, L. Polimeno, A. Rizzo, B. L. Rosa, G. Cruciani, L. Dominici, M. De Giorgi, and G. Gigli, "Tunable out-of-plane excitons in 2D single-crystal perovskites," ACS Photon. **5**, 4179–4185 (2018).
34. R. A. DeCrescent, N. R. Venkatesan, C. J. Dahlman, R. M. Kennard, M. L. Chabinyc, and J. A. Schuller, "Optical constants and effective-medium origins of large optical anisotropies in layered hybrid organic/inorganic perovskites," ACS Nano **13**, 10745–10753 (2019).
35. Z. Guo, X. Wu, T. Zhu, X. Zhu, and L. Huang, "Electron-phonon scattering in atomically thin 2D perovskites," ACS Nano **10**, 9992–9998 (2016).
36. S. Neutzner, F. Thouin, D. Cortecchia, A. Petrozza, C. Silva, and A. R. S. Kandada, "Exciton-polaron spectral structures in two-dimensional hybrid lead-halide perovskites," Phys. Rev. Mater. **2**, 064605 (2018).
37. J. Nishida, J. P. Breen, K. P. Lindquist, D. Umeyama, H. I. Karunadasa, and M. D. Fayer, "Dynamically disordered lattice in a layered Pb-I-SCN perovskite thin film probed by two-dimensional infrared spectroscopy," J. Am. Chem. Soc. **140**, 9882–9890 (2018).
38. L. Ni, U. Huynh, A. Cheminal, T. H. Thomas, R. Shivanna, T. F. Hinrichsen, S. Ahmad, A. Sadhanala, and A. Rao, "Real-time observation of exciton-phonon coupling dynamics in self-assembled hybrid perovskite quantum wells," ACS Nano **11**, 10834–10843 (2017).
39. D. B. Straus, S. Hurtado Parra, N. Iotov, J. Gebhardt, A. M. Rappe, J. E. Subotnik, J. M. Kikkawa, and C. R. Kagan, "Direct observation of electron-phonon coupling and slow vibrational relaxation in organic-inorganic hybrid perovskites," J. Am. Chem. Soc. **138**, 13798–13801 (2016).
40. F. Thouin, D. A. Valverde-Chávez, C. Quarti, D. Cortecchia, I. Bargigia, D. Beljonne, A. Petrozza, C. Silva, and A. R. S. Kandada, "Phonon coherences reveal the polaronic character of excitons in two-dimensional lead halide perovskites," Nat. Mater. **18**, 349–356 (2019).
41. P. Guo, C. C. Stoumpos, L. Mao, S. Sadasivam, J. B. Ketterson, P. Darancet, M. G. Kanatzidis, and R. D. Schaller, "Cross-plane coherent acoustic phonons in two-dimensional organic-inorganic hybrid perovskites," Nat. Commun. **9**, 2019 (2018).
42. X. Gong, O. Voznyy, A. Jain, W. Liu, R. Sabatini, Z. Piontkowski, G. Walters, G. Bappi, S. Nokhrin, and O. Bushuyev, "Electron-phonon interaction in efficient perovskite blue emitters," Nat. Mater. **17**, 550–556 (2018).
43. M. D. Smith, A. Jaffe, E. R. Dohner, A. M. Lindenberg, and H. I. Karunadasa, "Structural origins of broadband emission from layered Pb-Br hybrid perovskites," Chem. Sci. **8**, 4497–4504 (2017).
44. D. Cortecchia, S. Neutzner, A. R. Srimath Kandada, E. Mosconi, D. Meggiolaro, F. De Angelis, C. Soci, and A. Petrozza, "Broadband emission in two-dimensional hybrid perovskites: the role of structural deformation," J. Am. Chem. Soc. **139**, 39–42 (2017).
45. T. Hu, M. D. Smith, E. R. Dohner, M.-J. Sher, X. Wu, M. T. Trinh, A. Fisher, J. Corbett, X.-Y. Zhu, and H. I. Karunadasa, "Mechanism for broadband white-light emission from two-dimensional (110) hybrid perovskites," J. Phys. Chem. Lett. **7**, 2258–2263 (2016).
46. D. O'carroll, I. Lieberwirth, and G. Redmond, "Microcavity effects and optically pumped lasing in single conjugated polymer nanowires," Nat. Nanotechnol. **2**, 180–184 (2007).
47. H. H. Fang, R. Ding, S. Y. Lu, Y. D. Yang, Q. D. Chen, J. Feng, Y. Z. Huang, and H. B. Sun, "Whispering-gallery mode lasing from patterned molecular single-crystalline microcavity array," Laser Photon. Rev. **7**, 281–288 (2013).
48. S. Noda, F. T. Mahi, and H. Zappe, "Photonic crystals," in *Reference Module in Materials Science and Materials Engineering* (Elsevier, 2016), pp. 1–11.
49. G. Panzarini, L. C. Andreani, A. Armitage, D. Baxter, M. Skolnick, V. Astratov, J. Roberts, A. V. Kavokin, M. R. Vladimirova, and M. Kaliteevski, "Cavity-polariton dispersion and polarization splitting in single and coupled semiconductor microcavities," Phys. Solid State **41**, 1223–1238 (1999).
50. Y. Liu, Y. Zhang, Z. Yang, H. Ye, J. Feng, Z. Xu, X. Zhang, R. Munir, J. Liu, P. Zuo, Q. Li, M. Hu, L. Meng, K. Wang, D.-M. Smilgies, G. Zhao, H. Xu, Z. Yang, A. Amassian, J. Li, K. Zhao, and S. Liu, "Multi-inch single-crystalline perovskite membrane for high-detectivity flexible photosensors," Nat. Commun. **9**, 5302 (2018).
51. Y. Zhang, Y. Liu, Z. Xu, H. Ye, Q. Li, M. Hu, Z. Yang, and S. Liu, "Two-dimensional $(PEA)_2PbBr_4$ perovskite single crystals for a high performance UV-detector," J. Mater. Chem. C **7**, 1584–1591 (2019).
52. Y. Hassan, Y. Song, R. D. Pensack, A. I. Abdelrahman, Y. Kobayashi, M. A. Winnik, and G. D. Scholes, "Structure-tuned lead halide perovskite nanocrystals," Adv. Mater. **28**, 566–573 (2016).
53. D. Ghoshal, T. Wang, H. Z. Tsai, S. W. Chang, M. Crommie, N. Koratkar, and S. F. Shi, "Catalyst-free and morphology-controlled growth of 2D perovskite nanowires for polarized light detection," Adv. Opt. Mater. **7**, 1900039 (2019).
54. A. Kooijman, L. A. Muscarella, and R. M. Williams, "Perovskite thin film materials stabilized and enhanced by zinc (II) doping," Appl. Sci. **9**, 1678 (2019).
55. S. Wang, F. Yang, J. Zhu, Q. Cao, Y. Zhong, A. Wang, W. Du, and X. Liu, "Growth of metal halide perovskite materials," Sci. China Mater. **63**, 1438–1463 (2020).
56. X. Zhang, H. Shi, H. Dai, X. Zhang, X. W. Sun, and Z. Zhang, "Exciton-polariton properties in planar microcavity of millimeter-sized two-dimensional perovskite sheet," ACS Appl. Mater. Interfaces **12**, 5081–5089 (2020).
57. C. M. Raghavan, T.-P. Chen, S.-S. Li, W.-L. Chen, C.-Y. Lo, Y.-M. Liao, G. Haider, C.-C. Lin, C.-C. Chen, and R. Sankar, "Low-threshold lasing from 2D homologous organic-inorganic hybrid Ruddlesden-Popper perovskite single crystals," Nano Lett. **18**, 3221–3228 (2018).
58. A. Brehier, R. Parashkov, J. S. Lauret, and E. Deleporte, "Strong exciton-photon coupling in a microcavity containing layered perovskite semiconductors," Appl. Phys. Lett. **89**, 171110 (2006).
59. Z. Han, H.-S. Nguyen, F. Boitier, Y. Wei, K. Abdel-Baki, J.-S. Lauret, J. Bloch, S. Bouchoule, and E. Deleporte, "High-*Q* planar organic-inorganic perovskite-based microcavity," Opt. Lett. **37**, 5061–5063 (2012).
60. J. Wang, R. Su, J. Xing, D. Bao, C. Diederichs, S. Liu, T. C. Liew, Z. Chen, and Q. Xiong, "Room temperature coherently coupled exciton-polaritons in two-dimensional organic-inorganic perovskite," ACS Nano **12**, 8382–8389 (2018).
61. H. Zhang, Q. Liao, Y. Wu, Z. Zhang, Q. Gao, P. Liu, M. Li, J. Yao, and H. Fu, "2D Ruddlesden-Popper perovskites microring laser array," Adv. Mater. **30**, 1706186 (2018).
62. N. H. M. Dang, D. Gerace, E. Drouard, G. Trippé-Allard, F. Lédée, R. Mazurczyk, E. Deleporte, C. Seassal, and H. S. Nguyen, "Tailoring dispersion of room-temperature exciton-polaritons with perovskite-based subwavelength metasurfaces," Nano Lett. **20**, 2113–2119 (2020).
63. H. Dong, C. Zhang, X. Liu, J. Yao, and Y. S. Zhao, "Materials chemistry and engineering in metal halide perovskite lasers," Chem. Soc. Rev. **49**, 951–982 (2020).
64. C. C. Stoumpos, D. H. Cao, D. J. Clark, J. Young, J. M. Rondinelli, J. I. Jang, J. T. Hupp, and M. G. Kanatzidis, "Ruddlesden-Popper hybrid lead iodide perovskite 2D homologous semiconductors," Chem. Mater. **28**, 2852–2867 (2016).
65. K. Leng, I. Abdelwahab, I. Verzhbitskiy, M. Telychko, L. Chu, W. Fu, X. Chi, N. Guo, Z. Chen, and Z. Chen, "Molecularly thin two-dimensional hybrid perovskites with tunable optoelectronic properties due to reversible surface relaxation," Nat. Mater. **17**, 908–914 (2018).
66. K. Tanaka and T. Kondo, "Bandgap and exciton binding energies in lead-iodide-based natural quantum-well crystals," Sci. Technol. Adv. Mater. **4**, 599–604 (2003).
67. T. Dammak, S. Elleuch, H. Bougzhala, A. Mlayah, R. Chtourou, and Y. Abid, "Synthesis, vibrational and optical properties of a new three-layered organic-inorganic perovskite $(C_4H_9NH_3)_4Pb_3I_4Br_6$," J. Lumin. **129**, 893–897 (2009).
68. L. Dou, A. B. Wong, Y. Yu, M. Lai, N. Kornienko, S. W. Eaton, A. Fu, C. G. Bischak, J. Ma, T. Ding, N. S. Ginsberg, L.-W. Wang, A. P. Alivisatos, and P. Yang, "Atomically thin two-dimensional organic-inorganic hybrid perovskites," Science **349**, 1518–1521 (2015).
69. E. Shi, B. Yuan, S. B. Shiring, Y. Gao, Akriti, Y. Guo, C. Su, M. Lai, P. Yang, J. Kong, B. M. Savoie, Y. Yu, and L. Dou, "Two-dimensional

halide perovskite lateral epitaxial heterostructures," Nature **580**, 614–620 (2020).
70. D. Ma, Y. Fu, L. Dang, J. Zhai, I. A. Guzei, and S. Jin, "Single-crystal microplates of two-dimensional organic-inorganic lead halide layered perovskites for optoelectronics," Nano Res. **10**, 2117–2129 (2017).
71. W. Niu, L. A. Ibbotson, D. Leipold, E. Runge, G. V. Prakash, and J. J. Baumberg, "Image excitons and plasmon-exciton strong coupling in two-dimensional perovskite semiconductors," Phys. Rev. B **91**, 161303 (2015).
72. F. Meinardi, A. Colombo, K. A. Velizhanin, R. Simonutti, M. Lorenzon, L. Beverina, R. Viswanatha, V. I. Klimov, and S. Brovelli, "Large-area luminescent solar concentrators based on 'Stokes-shift-engineered' nanocrystals in a mass-polymerized PMMA matrix," Nat. Photonics **8**, 392–399 (2014).
73. L. Protesescu, S. Yakunin, M. I. Bodnarchuk, F. Krieg, R. Caputo, C. H. Hendon, R. X. Yang, A. Walsh, and M. V. Kovalenko, "Nanocrystals of cesium lead halide perovskites ($CsPbX_3$, X= Cl, Br, and I): novel optoelectronic materials showing bright emission with wide color gamut," Nano Lett. **15**, 3692–3696 (2015).
74. L.-C. Chen, C.-H. Tien, Z.-L. Tseng, Y.-S. Dong, and S. Yang, "Influence of PMMA on all-inorganic halide perovskite $CsPbBr_3$ quantum dots combined with polymer matrix," Materials **12**, 985 (2019).
75. L. Wang, L. Meng, L. Chen, S. Huang, X. Wu, G. Dai, L. Deng, J. Han, B. Zou, C. Zhang, and H. Zhong, "Ultralow-threshold and color-tunable continuous-wave lasing at room-temperature from in situ fabricated perovskite quantum dots," J. Phys. Chem. Lett. **10**, 3248–3253 (2019).
76. H. Tsai, W. Nie, J.-C. Blancon, C. C. Stoumpos, R. Asadpour, B. Harutyunyan, A. J. Neukirch, R. Verduzco, J. J. Crochet, and S. Tretiak, "High-efficiency two-dimensional Ruddlesden-Popper perovskite solar cells," Nature **536**, 312–316 (2016).
77. H. Zhang, Y. Wu, Q. Liao, Z. Zhang, Y. Liu, Q. Gao, P. Liu, M. Li, J. Yao, and H. Fu, "A two-dimensional Ruddlesden-Popper perovskite nanowire laser array based on ultrafast light-harvesting quantum wells," Angew. Chem. **130**, 7874–7878 (2018).
78. D. I. Babic and S. W. Corzine, "Analytic expressions for the reflection delay, penetration depth, and absorptance of quarter-wave dielectric mirrors," IEEE J. Quantum Electron. **28**, 514–524 (1992).
79. H. K. H. Choy, *Design and Fabrication of Distributed Bragg Reflectors for Vertical-Cavity Surface-Emitting Lasers* (Massachusetts Institute of Technology, 1998).
80. A. Brehier, R. Parashkov, J.-S. Lauret, and E. Deleporte, "Strong exciton-photon coupling in a microcavity containing layered perovskite semiconductors," Appl. Phys. Lett. **89**, 171110 (2006).
81. G. Lanty, A. Brehier, R. Parashkov, J.-S. Lauret, and E. Deleporte, "Strong exciton-photon coupling at room temperature in microcavities containing two-dimensional layered perovskite compounds," New J. Phys. **10**, 065007 (2008).
82. C. Weisbuch, M. Nishioka, A. Ishikawa, and Y. Arakawa, "Observation of the coupled exciton-photon mode splitting in a semiconductor quantum microcavity," Phys. Rev. Lett. **69**, 3314–3317 (1992).
83. M. Brodin and M. Matsko, "Polariton effects in luminescence from ZnTe crystals: surface and bulk polaritons," Solid State Commun. **35**, 375–377 (1980).
84. R. André, D. Heger, L. S. Dang, and Y. M. d'Aubigné, "Spectroscopy of polaritons in CdTe-based microcavities," J. Cryst. Growth **184**, 758–762 (1998).
85. H. Mathieu, Y. Chen, J. Camassel, J. Allegre, and D. Robertson, "Excitons and polaritons in InP," Phys. Rev. B **32**, 4042–4051 (1985).
86. G. Malpuech, A. Di Carlo, A. Kavokin, J. J. Baumberg, M. Zamfirescu, and P. Lugli, "Room-temperature polariton lasers based on GaN microcavities," Appl. Phys. Lett. **81**, 412–414 (2002).
87. Y.-Y. Lai, Y.-P. Lan, and T.-C. Lu, "Strong light-matter interaction in ZnO microcavities," Light Sci. Appl. **2**, e76 (2013).
88. J.-H. Song, "Optical properties of GaN and ZnO," in *Oxide and Nitride Semiconductors: Processing, Properties, and Applications*, T. Yao and S.-K. Hong, eds. (Springer, 2009), pp. 311–354.
89. M. Litinskaya, "Exciton polariton kinematic interaction in crystalline organic microcavities," Phys. Rev. B **77**, 155325 (2008).
90. Y. Zhang, C.-K. Lim, Z. Dai, G. Yu, J. W. Haus, H. Zhang, and P. N. Prasad, "Photonics and optoelectronics using nano-structured hybrid perovskite media and their optical cavities," Phys. Rep. **795**, 1–51 (2019).
91. S. Zhang, Q. Shang, W. Du, J. Shi, Z. Wu, Y. Mi, J. Chen, F. Liu, Y. Li, M. Liu, Q. Zhang, and X. Liu, "Strong exciton-photon coupling in hybrid inorganic-organic perovskite micro/nanowires," Adv. Opt. Mater. **6**, 1701032 (2018).
92. W. Du, S. Zhang, J. Shi, J. Chen, Z. Wu, Y. Mi, Z. Liu, Y. Li, X. Sui, R. Wang, X. Qiu, T. Wu, Y. Xiao, Q. Zhang, and X. Liu, "Strong exciton-photon coupling and lasing behavior in all-inorganic $CsPbBr_3$ micro/nanowire Fabry-Pérot cavity," ACS Photon. **5**, 2051–2059 (2018).
93. Q. Han, J. Wang, J. Lu, L. Sun, F. Lyu, H. Wang, Z. Chen, and Z. Wang, "Transition between exciton-polariton and coherent photonic lasing in all-inorganic perovskite microcuboid," ACS Photon. **7**, 454–462 (2020).
94. Q. Shang, C. Li, S. Zhang, Y. Liang, Z. Liu, X. Liu, and Q. Zhang, "Enhanced optical absorption and slowed light of reduced-dimensional $CsPbBr_3$ nanowire crystal by exciton-polariton," Nano Lett. **20**, 1023–1032 (2020).
95. R. Su, C. Diederichs, J. Wang, T. C. H. Liew, J. Zhao, S. Liu, W. Xu, Z. Chen, and Q. Xiong, "Room-temperature polariton lasing in all-inorganic perovskite nanoplatelets," Nano Lett. **17**, 3982–3988 (2017).
96. S. Zhang, J. Chen, J. Shi, L. Fu, W. Du, X. Sui, Y. Mi, Z. Jia, F. Liu, and J. Shi, "Trapped exciton-polariton condensate by spatial confinement in a perovskite microcavity," ACS Photon. **7**, 327–337 (2020).
97. W. Du, S. Zhang, Q. Zhang, and X. Liu, "Recent progress of strong exciton-photon coupling in lead halide perovskites," Adv. Mater. **31**, 1804894 (2019).
98. T. J. S. Evans, A. Schlaus, Y. Fu, X. Zhong, T. L. Atallah, M. S. Spencer, L. E. Brus, S. Jin, and X. Y. Zhu, "Continuous-wave lasing in cesium lead bromide perovskite nanowires," Adv. Opt. Mater. **6**, 1700982 (2018).
99. Q. Shang, M. Li, L. Zhao, D. Chen, S. Zhang, S. Chen, P. Gao, C. Shen, J. Xing, G. Xing, B. Shen, X. Liu, and Q. Zhang, "Role of the exciton-polariton in a continuous-wave optically pumped $CsPbBr_3$ perovskite laser," Nano Lett. **20**, 6636–6646 (2020).
100. T. Fujita, Y. Sato, T. Kuitani, and T. Ishihara, "Tunable polariton absorption of distributed feedback microcavities at room temperature," Phys. Rev. B **57**, 12428–12434 (1998).
101. K. Pradeesh, J. Baumberg, and G. V. Prakash, "Strong exciton-photon coupling in inorganic-organic multiple quantum wells embedded low-Q microcavity," Opt. Express **17**, 22171–22178 (2009).
102. A. Fieramosca, L. Polimeno, V. Ardizzone, L. De Marco, M. Pugliese, V. Maiorano, M. De Giorgi, L. Dominici, G. Gigli, and D. Gerace, "Two-dimensional hybrid perovskites sustaining strong polariton interactions at room temperature," Sci. Adv. **5**, eaav9967 (2019).
103. P. M. Walker, L. Tinkler, D. V. Skryabin, A. Yulin, B. Royall, I. Farrer, D. A. Ritchie, M. S. Skolnick, and D. N. Krizhanovskii, "Ultra-low-power hybrid light-matter solitons," Nat. Commun. **6**, 8317 (2015).
104. L. K. Van Vugt, B. Piccione, and R. Agarwal, "Incorporating polaritonic effects in semiconductor nanowire waveguide dispersion," Appl. Phys. Lett. **97**, 061115 (2010).
105. M. Vladimirova, S. Cronenberger, D. Scalbert, K. Kavokin, A. Miard, A. Lemaître, J. Bloch, D. Solnyshkov, G. Malpuech, and A. Kavokin, "Polariton-polariton interaction constants in microcavities," Phys. Rev. B **82**, 075301 (2010).
106. L. Polimeno, A. Fieramosca, G. Lerario, M. Cinquino, M. De Giorgi, D. Ballarini, F. Todisco, L. Dominici, V. Ardizzone, M. Pugliese, C. T. Prontera, V. Maiorano, G. Gigli, L. De Marco, and D. Sanvitto, "Observation of two thresholds leading to polariton condensation in 2D hybrid perovskites," Adv. Opt. Mater. **8**, 2000176 (2020).
107. J. Chen, W. Du, J. Shi, M. Li, Y. Wang, Q. Zhang, and X. Liu, "Perovskite quantum dot lasers," InfoMat **2**, 170–183 (2020).
108. Y. Mi, Y. Zhong, Q. Zhang, and X. Liu, "Continuous-wave pumped perovskite lasers," Adv. Opt. Mater. **7**, 1900544 (2019).
109. Q. Zhang, R. Su, W. Du, X. Liu, L. Zhao, S. T. Ha, and Q. Xiong, "Advances in small perovskite-based lasers," Small Methods **1**, 1700163 (2017).

110. C. Li, Z. Liu, Q. Shang, and Q. Zhang, "Surface-plasmon-assisted metal halide perovskite small lasers," Adv. Opt. Mater. **7**, 1900279 (2019).
111. G. Xing, N. Mathews, S. S. Lim, N. Yantara, X. Liu, D. Sabba, M. Grätzel, S. Mhaisalkar, and T. C. Sum, "Low-temperature solution-processed wavelength-tunable perovskites for lasing," Nat. Mater. **13**, 476–480 (2014).
112. T. Kondo, T. Azuma, T. Yuasa, and R. Ito, "Biexciton lasing in the layered perovskite-type material $(C_6H_{13}NH_3)_2PbI_4$," Solid State Commun. **105**, 253–255 (1998).
113. G. Grancini and M. K. Nazeeruddin, "Dimensional tailoring of hybrid perovskites for photovoltaics," Nat. Rev. Mater. **4**, 4–22 (2019).
114. M. Saba, F. Quochi, A. Mura, and G. Bongiovanni, "Excited state properties of hybrid perovskites," Acc. Chem. Res. **49**, 166–173 (2016).
115. M. N. Saha and A. Fowler, "On a physical theory of stellar spectra," Proc. R. Soc. London Series A **99**, 135–153 (1921).
116. J. S. Manser, J. A. Christians, and P. V. Kamat, "Intriguing optoelectronic properties of metal halide perovskites," Chem. Rev. **116**, 12956–13008 (2016).
117. M. Saba, M. Cadelano, D. Marongiu, F. Chen, V. Sarritzu, N. Sestu, C. Figus, M. Aresti, R. Piras, and A. G. Lehmann, "Correlated electron-hole plasma in organometal perovskites," Nat. Commun. **5**, 5049 (2014).
118. A. P. Schlaus, M. S. Spencer, and X. Zhu, "Light-matter interaction and lasing in lead halide perovskites," Acc. Chem. Res. **52**, 2950–2959 (2019).
119. W. Du, S. Zhang, Z. Wu, Q. Shang, Y. Mi, J. Chen, C. Qin, X. Qiu, Q. Zhang, and X. Liu, "Unveiling lasing mechanism in $CsPbBr_3$ microsphere cavities," Nanoscale **11**, 3145–3153 (2019).
120. D. Marongiu, M. Saba, F. Quochi, A. Mura, and G. Bongiovanni, "The role of excitons in 3D and 2D lead halide perovskites," J. Mater. Chem. C **7**, 12006–12018 (2019).
121. M. Li, Q. Gao, P. Liu, Q. Liao, H. Zhang, J. Yao, W. Hu, Y. Wu, and H. Fu, "Amplified spontaneous emission based on 2D Ruddlesden-Popper perovskites," Adv. Func. Mater. **28**, 1707006 (2018).
122. B. R. Sutherland, S. Hoogland, M. M. Adachi, C. T. Wong, and E. H. Sargent, "Conformal organohalide perovskites enable lasing on spherical resonators," ACS Nano **8**, 10947–10952 (2014).
123. W. K. Chong, K. Thirumal, D. Giovanni, T. W. Goh, X. Liu, N. Mathews, S. Mhaisalkar, and T. C. Sum, "Dominant factors limiting the optical gain in layered two-dimensional halide perovskite thin films," Phys. Chem. Chem. Phys. **18**, 14701–14708 (2016).
124. Z. Liu, "Research progress of low-dimensional metal halide perovskites for lasing applications," Chin. Phys. B **27**, 114209 (2018).
125. G. Xing, B. Wu, X. Wu, M. Li, B. Du, Q. Wei, J. Guo, E. K. Yeow, T. C. Sum, and W. Huang, "Transcending the slow bimolecular recombination in lead-halide perovskites for electroluminescence," Nat. Commun. **8**, 14558 (2017).
126. H. Cao, Y. Zhao, S.-T. Ho, E. Seelig, Q. Wang, and R. P. Chang, "Random laser action in semiconductor powder," Phys. Rev. Lett. **82**, 2278–2281 (1999).
127. M. Leonetti, C. Conti, and C. Lopez, "The mode-locking transition of random lasers," Nat. Photonics **5**, 615–617 (2011).
128. A. Baranov and E. Tournié, *Semiconductor Lasers: Fundamentals and Applications* (Elsevier, 2013).
129. Q. Liao, K. Hu, H. Zhang, X. Wang, J. Yao, and H. Fu, "Perovskite microdisk microlasers self-assembled from solution," Adv. Mater. **27**, 3405–3410 (2015).
130. W. Zhang, L. Peng, J. Liu, A. Tang, J. S. Hu, J. Yao, and Y. S. Zhao, "Controlling the cavity structures of two-photon-pumped perovskite microlasers," Adv. Mater. **28**, 4040–4046 (2016).
131. C. J. Chang-Hasnain, "Tunable VCSEL," IEEE J. Sel. Top. Quantum Electron. **6**, 978–987 (2000).
132. S. Chen, C. Zhang, J. Lee, J. Han, and A. Nurmikko, "High-*Q*, low-threshold monolithic perovskite thin-film vertical-cavity lasers," Adv. Mater. **29**, 1604781 (2017).
133. Y. Wang, X. Li, V. Nalla, H. Zeng, and H. Sun, "Solution-processed low threshold vertical cavity surface emitting lasers from all-inorganic perovskite nanocrystals," Adv. Func. Mater. **27**, 1605088 (2017).
134. E. P. Booker, M. B. Price, P. J. Budden, H. Abolins, Y. del Valle-Inclan Redondo, L. Eyre, I. Nasrallah, R. T. Phillips, R. H. Friend, and F. Deschler, "Vertical cavity biexciton lasing in 2D dodecylammonium lead iodide perovskites," Adv. Opt. Mater. **6**, 1800616 (2018).
135. Y. Fu, H. Zhu, J. Chen, M. P. Hautzinger, X.-Y. Zhu, and S. Jin, "Metal halide perovskite nanostructures for optoelectronic applications and the study of physical properties," Nat. Rev. Mater. **4**, 169–188 (2019).
136. W. Liu, X. Li, Y. Song, C. Zhang, X. Han, H. Long, B. Wang, K. Wang, and P. Lu, "Cooperative enhancement of two-photon-absorption-induced photoluminescence from a 2D perovskite-microsphere hybrid dielectric structure," Adv. Funct. Mater. **28**, 1707550 (2018).
137. H. Yang, R. Trouillon, G. Huszka, and M. A. Gijs, "Super-resolution imaging of a dielectric microsphere is governed by the waist of its photonic nanojet," Nano Lett. **16**, 4862–4870 (2016).
138. Y. Yan, Y. Zeng, Y. Wu, Y. Zhao, L. Ji, Y. Jiang, and L. Li, "Ten-fold enhancement of ZnO thin film ultraviolet-luminescence by dielectric microsphere arrays," Opt. Express **22**, 23552–23564 (2014).
139. Y. Dong, Y. Gu, Y. Zou, J. Song, L. Xu, J. Li, J. Xue, X. Li, and H. Zeng, "Improving all-inorganic perovskite photodetectors by preferred orientation and plasmonic effect," Small **12**, 5622–5632 (2016).
140. B. Du, W. Yang, Q. Jiang, H. Shan, D. Luo, B. Li, W. Tang, F. Lin, B. Shen, and Q. Gong, "Plasmonic-functionalized broadband perovskite photodetector," Adv. Opt. Mater. **6**, 1701271 (2018).
141. C.-K. Lim, Q. Li, T. Zhang, T. Thomay, A. N. Cartwright, M. T. Swihart, and P. N. Prasad, "Enhanced fatigue resistance of suppressed hysteresis in perovskite solar cells by an organic cross-linker," Sol. Energy Mater. Sol. Cells **176**, 30–35 (2018).
142. A. Furasova, E. Calabró, E. Lamanna, E. Tiguntseva, E. Ushakova, E. Ubyivovk, V. Mikhailovskii, A. Zakhidov, S. Makarov, and A. Di Carlo, "Resonant silicon nanoparticles for enhanced light harvesting in halide perovskite solar cells," Adv. Opt. Mater. **6**, 1800576 (2018).
143. J. Feng, C. Gong, H. Gao, W. Wen, Y. Gong, X. Jiang, B. Zhang, Y. Wu, Y. Wu, H. Fu, L. Jiang, and X. Zhang, "Single-crystalline layered metal-halide perovskite nanowires for ultrasensitive photodetectors," Nat. Electron. **1**, 404–410 (2018).
144. J. Bao and V. G. Hadjiev, "Origin of luminescent centers and edge states in low-dimensional lead halide perovskites: controversies, challenges and instructive approaches," Nano-Micro Lett. **11**, 26 (2019).
145. B. Piccione, C.-H. Cho, L. K. van Vugt, and R. Agarwal, "All-optical active switching in individual semiconductor nanowires," Nat. Nanotechnol. **7**, 640–645 (2012).
146. X. Guo, Y. Ying, and L. Tong, "Photonic nanowires: from subwavelength waveguides to optical sensors," Acc. Chem. Res. **47**, 656–666 (2014).
147. S. Kim and R. Yan, "Recent developments in photonic, plasmonic and hybrid nanowire waveguides," J. Mater. Chem. C **6**, 11795–11816 (2018).
148. Y. Dong, Y. Zhang, X. Li, Y. Feng, H. Zhang, and J. Xu, "Chiral perovskites: promising materials toward next-generation optoelectronics," Small **15**, 1902237 (2019).